

# Parity-violating photon circular polarization in $nd \rightarrow {}^3H\gamma$ with effective field theory at thermal energy

M. Moeini Arani\* and S. Bayegan†

*Department of Physics, University of Tehran, P.O.Box 14395-547, Tehran, Iran*

(Dated: February 18, 2022)

## Abstract

We study the parity-violating effects in  $nd \rightarrow {}^3H\gamma$  process using pionless effective field theory (EFT( $\not{\pi}$ )) at thermal energy. For the weak  $NN$  interaction the parity-violating Lagrangian contains five independent low-energy coupling constants (LECs). One can fix the coupling constants by comparison of the calculated observables with a sufficient number of experimental data. So, we need five observables to obtain LECs. One of the five parity-violating observables is the photon circular polarization ( $P_\gamma$ ) in  $nd \rightarrow {}^3H\gamma$  process. We calculate  $P_\gamma$  at the leading order in terms of LECs. We compare our results with the previous  $P_\gamma$  calculation based on the model of Desplanques, Donoghue, and Holstein.

PACS numbers: 11.10.-z; 21.45.+v; 21.10.Hw; 25.40.Lw; 21.30.Fe

---

\*Electronic address: m.moeini.a@khayam.ut.ac.ir (corresponding author)

†Electronic address: bayegan@khayam.ut.ac.ir

## I. INTRODUCTION

The Effective Field Theory (EFT) approach provides a systematic and model-independent framework to analyse the hadronic parity-violating (PV) effects in few-body system [1, 2]. We use the pionless effective field theory (EFT( $\not{\pi}$ )) for the PV process which is at the energies well below the pion production threshold.

Recently, the leading-order (LO) PV nucleon-nucleon ( $NN$ ) Lagrangian has been expressed in a variety of bases [3, 4]. The LO PV Lagrangian in the partial-wave basis is written in terms of five independent unknown coupling constants corresponding to five different S-P wave combinations. This Lagrangian has been applied for neutron-neutron, proton-proton and neutron-proton longitudinal asymmetries without dibaryon fields in EFT( $\not{\pi}$ ) [3].

The calculation of  $P_\gamma$  in  $np \rightarrow d\gamma$  at threshold was introduced with the PV dibaryon-nucleon-nucleon ( $dNN$ ) Lagrangian in EFT( $\not{\pi}$ ). The PV  $dNN$  Lagrangian is constructed in terms of three weak coupling constants. In fact, parts of the PV Lagrangian in dibaryon formalism are given by this Lagrangian structure. Result for  $P_\gamma$  was obtained in terms of two unknown weak  $dNN$  coupling constants for the parity mixing in the spin-singlet and spin-triplet states [5].

The photon asymmetry  $A_\gamma$  and circular polarization  $P_\gamma$  in  $np \rightarrow d\gamma$  process were also derived using the PV  $NN$  lagrangian based on the partial-wave basis with and without dibaryon fields. EFT( $\not{\pi}$ ) with dibaryon fields has proven to be convenient for few-nucleon systems at low energies [6].

In the three-body sector, a systematic analysis of the parity-conserving (PC)  $nd \rightarrow {}^3H\gamma$  process at threshold was carried out using the EFT( $\not{\pi}$ ) [7, 8]. In the present work, we concentrate on the PV  $nd \rightarrow {}^3H\gamma$  amplitude. We will make predictions for the PV observable in  $nd \rightarrow {}^3H\gamma$  process with the PV Lagrangian based on the five independent LECs in the dibaryon EFT( $\not{\pi}$ ).

The analysis of the PV three-nucleon interaction (3NI) and calculation of neutron-proton and neutron-deuteron spin rotation have been performed in the EFT( $\not{\pi}$ ) framework. The results show that no PV 3NI enters at LO or next-to-leading order (NLO) in the nucleon-deuteron ( $Nd$ ) system [9, 10]. According to these results we adopt the PV Lagrangian for the two-nucleon interaction in the present calculation.

Theoretical calculations of the PV photon asymmetry and circular polarization of the

outgoing photon in  $nd \rightarrow {}^3H\gamma$  process were previously performed with the potential model. These analyses were based on Desplanques, Donoghue, and Holstein (DDH) meson exchange potential. The calculated results were  $A_\gamma^t = 0.81 \times 10^{-6}$  and  $A_\gamma^t = 0.61 \times 10^{-6}$  for the two super-soft-core (SSC) and Reid-soft-core (RSC) potentials, respectively. The DDH calculation of  $P_\gamma$  was also given for the two SSC and RSC potentials,  $P_\gamma = -1.39 \times 10^{-6}$  and  $P_\gamma = -1.14 \times 10^{-6}$ , respectively [11]. Recently, the PV effects in  $nd \rightarrow {}^3H\gamma$  were calculated for DDH and EFT weak interaction potentials [12]. We compare these  $P_\gamma$  values with our results in sect.V.

Finally, the experimental observation for the PV photon asymmetry in  $nd \rightarrow {}^3H\gamma$  process was measured at ILL [13] and the result was presented as  $A_\gamma^t = (4.2 \pm 3.8) \times 10^{-6}$ . The experimental data for  $P_\gamma$  in this process has not been reported to this point at the thermal energy.

Our paper is organized as follows. In sect. II we present briefly the PC formalism for the  $Nd$  scattering and neutron-deuteron radiative capture. The PV  $Nd$  scattering and PV  $nd \rightarrow {}^3H\gamma$  processes are explained in sect. III. We obtain the PV amplitude of  $nd \rightarrow {}^3H\gamma$  process in sect. IIIB with the calculation of the appropriate diagrams. The numerical methods for the evaluation of the PC and PV amplitudes of  $nd \rightarrow {}^3H\gamma$  process are explained in sect. IV. In sect. V the results of  $P_\gamma$  in  $nd \rightarrow {}^3H\gamma$  are estimated and compared with the DDH framework. We summarize the paper and discuss extension of the investigation to other observable such as the PV photon asymmetry and other few-body systems in sect. VI.

## II. PARITY-CONSERVING SECTOR

In the study of the weak interaction effects, we calculate the observables which depend on the PV interactions. For this purpose the  $P_\gamma$  in  $nd \rightarrow {}^3H\gamma$  process is chosen. To this aim we need the PC amplitudes for both  $Nd$  scattering and  $nd \rightarrow {}^3H\gamma$  processes. We briefly describe below the procedure to obtain these two PC amplitudes at the leading order.

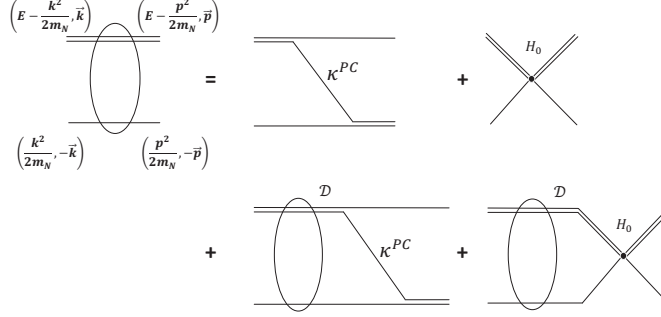


FIG. 1: The Faddeev equation for the  $Nd$  scattering. Single solid line denotes a nucleon. Double line is propagator of the two intermediate auxiliary fields  $d_s$  and  $d_t$ , denoted by  $\mathcal{D}$ .  $\mathcal{K}^{PC}$  and  $H_0$  are the propagator of exchanged nucleon and three-body interaction at LO, respectively.

### A. Parity-conserving $Nd$ scattering

We proceed by introducing the Lagrangian of two- and three-nucleon systems in  $Z$ -parametrization [14, 15]

$$\mathcal{L}^{PC} = \mathcal{L}^{PC}_{two\ body} + \mathcal{L}^{PC}_{three\ body}, \quad (1)$$

where

$$\begin{aligned} \mathcal{L}^{PC}_{two\ body} = & N^\dagger \left( i\partial_0 + \frac{\nabla^2}{2m_N} \right) N \\ & + d_s^{A\dagger} \left[ \Delta_s - c_{0s} \left( i\partial_0 + \frac{\nabla^2}{4m_N} + \frac{\gamma_s^2}{m_N} \right) \right] d_s^A \\ & + d_t^{i\dagger} \left[ \Delta_t - c_{0t} \left( i\partial_0 + \frac{\nabla^2}{4m_N} + \frac{\gamma_t^2}{m_N} \right) \right] d_t^i \\ & - y \left( d_s^{A\dagger} (N^\dagger P^A N) + h.c. \right) \\ & - y \left( d_t^{i\dagger} (N^\dagger P^i N) + h.c. \right) + \dots, \end{aligned} \quad (2)$$

$$\begin{aligned} \mathcal{L}^{PC}_{three\ body} = & \frac{m_N y^2 H_0(\Lambda)}{3\Lambda^2} \left( N^\dagger (d_t^i \sigma_i)^\dagger (d_t^i \sigma_i) N \right. \\ & \left. - [N^\dagger (d_t^i \sigma_i)^\dagger (d_s^A \tau_A) N + h.c.] \right. \\ & \left. + N^\dagger (d_s^A \tau_A)^\dagger (d_s^A \tau_A) N \right) + \dots, \end{aligned} \quad (3)$$

where  $N$  is the nucleon iso-doublet and the auxiliary fields  $d_s^A$  and  $d_t^i$  carry the quantum number of  $^1S_0$  di-nucleon and the deuteron, respectively. The projectors  $P^i$  and  $P^A$  are

defined by  $P^i = \frac{1}{\sqrt{8}}\sigma_2\sigma^i\tau_2$  and  $P^A = \frac{1}{\sqrt{8}}\sigma_2\tau_2\tau^A$  where  $A = 1, 2, 3$  and  $i = 1, 2, 3$  are isotriplet and vector indices, respectively.  $\tau^A(\sigma^i)$  are isospin (spin) pauli matrices.  $m_N$  is the nucleon mass and the three-nucleon interaction at the leading order is  $H_0(\Lambda)$  with cut-off  $\Lambda$ . The parameters  $\Delta_{s/t}$  are the mass differences between the dibaryons and two nucleons.

According to the naive dimensional analysis: the parameters  $\Delta_{s/t} \sim Q$ , with mass-dimension 1, are entered at LO; dimensionless parameters  $c_{0s/t} \sim Q^0$  first appear at NLO; since they are expressed with two powers of momentum,  $c_{0s/t}p^2 \sim Q^2$ , where  $Q$  is small momentum and appears in  $\frac{Q}{m_\pi}$  or  $\frac{Q}{\tilde{\Lambda}}$  as an expansion parameter ( $m_\pi$  the pion mass,  $\tilde{\Lambda}$  a symmetry breaking scale) in EFT( $\not{\pi}$ ). The parameters of the Lagrangians in eqs.(2) and (3) are fixed using Z-parametrization [15].  $d_{s/t}NN$  coupling constant is chosen as

$$y^2 = \frac{4\pi}{m_N}, \quad (4)$$

and the LO parameters  $\Delta_{s/t}$  are obtained from the poles of the  $NN$  S-wave scattering amplitude at  $i\gamma_{s/t}$ .

The physical observables are cutoff independent, so in the three-body systems at the leading order all-dependence on the cutoff as  $\Lambda \rightarrow \infty$  can be made to vanish by introducing  $H_0$ . We know that the  $H_0(\Lambda)$  is of order  $Q^{-2}$  [15, 16].

Neutron-deuteron scattering is shown schematically in fig.1. We denote the single straight line as a nucleon with the propagator  $\frac{i}{q_0 - \frac{q^2}{2m_N} + i\varepsilon}$ . The double line represents the dibaryon field with propagators for the singlet and triplet cases. They are given by

$$\mathcal{D}^{LO}(q_0, q) = \begin{pmatrix} D_t^{LO}(q_0, q) & 0 \\ 0 & D_s^{LO}(q_0, q) \end{pmatrix}, \quad (5)$$

where

$$D_{s(t)}^{LO}(q_0, q) = \frac{1}{\gamma_{s(t)} - \sqrt{\frac{q^2}{4} - m_N q_0} - i\varepsilon}, \quad (6)$$

where  $\gamma_s = \frac{1}{a_s}$ ,  $a_s$  is the scattering length in  $^1S_0$  state and  $\gamma_t$  is the binding momentum of the deuteron.

We work in the center of mass frame for the  $Nd$  scattering with  $\vec{k}$  denotes the initial (on-shell) relative momentum of the deuteron and the third nucleon, and  $\vec{p}$  is the final (off-shell) momentum. we use notation suggested by Griesshammer in [15].

For scattering in the quartet ( $S=\frac{3}{2}$ ) channel all spins are aligned and there is no three-body interaction in this channel because of the Pauli principle forbids the three nucleons to be at the same point in space. In this channel, the initial and final dibaryon fields have to be in the triplet channel. So, in this channel we have only the  $d_t N \rightarrow d_t N$  transition and the corresponding amplitude in the cluster-configuration space can be written as

$$\begin{aligned} \begin{pmatrix} t_q^{PC,(L)}(E; k, p) & 0 \\ 0 & 0 \end{pmatrix} &= -4\pi \mathcal{K}_{(L)}^{PC}(E, k, p) \begin{pmatrix} 1 & 0 \\ 0 & 0 \end{pmatrix} + \frac{2}{\pi} \int_0^\Lambda dq q^2 \mathcal{K}_{(L)}^{PC}(E, q, p) \\ &\times \begin{pmatrix} 1 & 0 \\ 0 & 0 \end{pmatrix} \mathcal{D}^{LO}(E - \frac{q^2}{2m_N}, q) \begin{pmatrix} t_q^{PC,(L)}(E; k, p) & 0 \\ 0 & 0 \end{pmatrix}. \end{aligned} \quad (7)$$

For the  $Nd$  scattering in the doublet ( $S=\frac{1}{2}$ ) channel, the parity-conserving amplitudes in cluster-configuration space are given by

$$\begin{aligned} \begin{pmatrix} t_{d_t N \rightarrow d_t N}^{PC,(L)}(E; k, p) & t_{d_s N \rightarrow d_t N}^{PC,(L)}(E; k, p) \\ t_{d_t N \rightarrow d_s N}^{PC,(L)}(E; k, p) & t_{d_s N \rightarrow d_s N}^{PC,(L)}(E; k, p) \end{pmatrix} &= \\ 2\pi \left[ \mathcal{K}_{(L)}^{PC}(E, k, p) \begin{pmatrix} 1 & -3 \\ -3 & 1 \end{pmatrix} + \delta_{L0} \mathcal{H}(E, \Lambda) \begin{pmatrix} 1 & -1 \\ -1 & 1 \end{pmatrix} \right] \\ - \frac{1}{\pi} \int_0^\Lambda dq q^2 \left[ \mathcal{K}_{(L)}^{PC}(E, q, p) \begin{pmatrix} 1 & -3 \\ -3 & 1 \end{pmatrix} + \delta_{L0} \mathcal{H}(E, \Lambda) \begin{pmatrix} 1 & -1 \\ -1 & 1 \end{pmatrix} \right] \\ \times \mathcal{D}^{LO}(E - \frac{q^2}{2m_N}, q) \begin{pmatrix} t_{d_t N \rightarrow d_t N}^{PC,(L)}(E; k, q) & t_{d_s N \rightarrow d_t N}^{PC,(L)}(E; k, q) \\ t_{d_t N \rightarrow d_s N}^{PC,(L)}(E; k, q) & t_{d_s N \rightarrow d_s N}^{PC,(L)}(E; k, q) \end{pmatrix}, \end{aligned} \quad (8)$$

where  $t_{d_x N \rightarrow d_y N}^{PC,(L)}$  denotes the  $d_x N \rightarrow d_y N$  transition amplitude ( $x, y = s$  or  $t$ ) in the doublet channel. The propagator of the exchanged nucleon,  $\mathcal{K}_{(L)}^{PC}$ , is

$$\mathcal{K}_{(L)}^{PC}(E, k, p) = \frac{1}{2} \int_{-1}^1 d(\cos\theta) \frac{P_L(\cos\theta)}{k^2 + p^2 - ME + kp \cos\theta}, \quad (9)$$

where  $P_L(x)$  denotes the  $L$ -th Legendre polynomial of the first kind and  $\theta$  indicates the angle between  $\vec{k}$  and  $\vec{p}$  vectors.  $\mathcal{H} = \frac{2H_0}{\Lambda^2} + \dots$  specifies the three-body force that renormalizes the amplitude and it is introduced for the S-wave ( $\delta_{L0}$ ).  $E = \frac{3\vec{k}^2}{4m_N} - \frac{\gamma_t^2}{m_N}$  is the total non-relativistic energy.

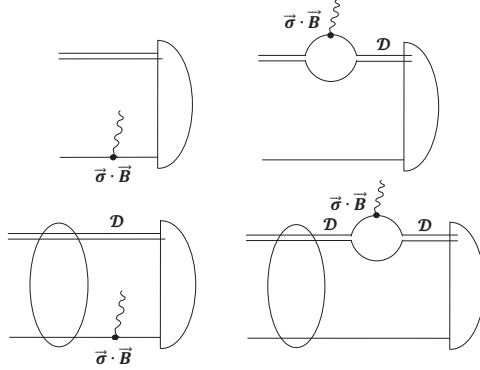


FIG. 2: The leading-order diagrams which contribute to PC (M1) amplitude of  $nd \rightarrow {}^3H\gamma$ . The small circles represent magnetic photon-Nucleon-Nucleon interaction. Wavy line shows a photon. Dashed oval and dashed half-oval indicate insertion of  $Nd$  scattering amplitude at LO from fig.1 and the formation of triton (the normalized triton wave function). Remaining notation as fig.1.

### B. Parity-conserving $nd \rightarrow {}^3H\gamma$ system

The dominated M1 amplitude of PC  $nd \rightarrow {}^3H\gamma$  process receives the contribution from the neutron and proton magnetic moment operators coupling to the magnetic field. At the leading order, the magnetic M1 interaction of the photon with the single nucleon is introduced by the Lagrangian

$$\mathcal{L}_B = \frac{e}{2m_N} N^\dagger (k_0 + k_1 \tau^3) \vec{\sigma} \cdot \vec{B} N, \quad (10)$$

where  $k_0 = \frac{1}{2}(k_p + k_n) = 0.4399$  and  $k_1 = \frac{1}{2}(k_p - k_n) = 2.35294$  are the isoscalar and isovector nucleon magnetic moments in the nuclear magnetons, respectively.  $k_p$  and  $k_n$  denote the proton and neutron magnetic moments, respectively.  $e$  is the electric charge and  $\vec{B}$  is magnetic field. The diagrams of PC  $nd \rightarrow {}^3H\gamma$  at LO are shown in fig.2. The dashed oval is the  $Nd$  scattering calculated in sect. II A. The dashed half-oval is the normalized triton wave function.

We note that for obtaining the normalized triton wave function, one should solve the homogeneous part of eq.(8) with application of  $E = -B_t$  where  $B_t$  is the binding energy of the triton. The wave function is then normalized using the nucleon and dibaryon propagators

as briefly explained in Appendix A. The homogeneous part of eq.(8) can be written as

$$t^{3H}(p) = -\frac{1}{\pi} \int_0^\Lambda dq q^2 \left[ \mathcal{K}_{(0)}^{PC}(-B_t, q, p) \begin{pmatrix} 1 & -3 \\ -3 & 1 \end{pmatrix} + \mathcal{H}(-B_t, \Lambda) \begin{pmatrix} 1 & -1 \\ -1 & 1 \end{pmatrix} \right] \\ \times \mathcal{D}^{LO}\left(-B_t - \frac{q^2}{2m_N}, q\right) t^{3H}(q), \quad (11)$$

where  $t^{3H}(q) = \begin{pmatrix} t_{d_t N \rightarrow d_t N}^{3H}(q) & t_{d_s N \rightarrow d_t N}^{3H}(q) \\ t_{d_t N \rightarrow d_s N}^{3H}(q) & t_{d_s N \rightarrow d_s N}^{3H}(q) \end{pmatrix}$ . Generally,  $t_{d_x N \rightarrow d_y N}^{3H}(q)$  denotes the contribution of the  $d_x N \rightarrow d_y N$  transition ( $x, y = s$  or  $t$ ) for making the triton.

For PC sector at the lowest order, we have two dominated M1 transitions, to which  ${}^3He$  and  ${}^3H$  belong,  $j^P = \frac{1}{2}^+ \rightarrow M1$  and  $j^P = \frac{3}{2}^+ \rightarrow M1$ . The following parametrization of the corresponding contributions to the matrix element are,

$$(t^\dagger \sigma_a N) (\vec{\varepsilon}_d \times (\vec{\varepsilon}_\gamma^* \times \vec{q}))_a, \quad i(t^\dagger N) (\vec{\varepsilon}_d \cdot \vec{\varepsilon}_\gamma^* \times \vec{q}), \quad (12)$$

with  $N$ ,  $t$ ,  $\vec{\varepsilon}_\gamma$ ,  $\vec{\varepsilon}_d$  and  $\vec{q}$  are the 2-component spinors of the initial nucleon field, the final  ${}^3H$  (or  ${}^3He$ ) field, the 3-vector polarization of the produced photon, the 3-vector polarization of the deuteron and the unit vector along the 3-momentum of the photons, respectively. For both possible magnetic transitions with  $j^P = \frac{1}{2}^+$  ( $\mathcal{W}^{PC}(2S_{\frac{1}{2}})$  amplitude) and  $j^P = \frac{3}{2}^+$  ( $\mathcal{W}^{PC}(4S_{\frac{3}{2}})$  amplitude) we can write

$$\mathcal{W}^{PC}(2S_{\frac{1}{2}}) [t^\dagger (i\vec{\varepsilon}_d \cdot \vec{\varepsilon}_\gamma^* \times \vec{q} + \vec{\sigma} \times \vec{\varepsilon}_d \cdot \vec{\varepsilon}_\gamma^* \times \vec{q}) N], \\ \mathcal{W}^{PC}(4S_{\frac{3}{2}}) [t^\dagger (i\vec{\varepsilon}_d \cdot \vec{\varepsilon}_\gamma^* \times \vec{q} + \vec{\sigma} \times \vec{\varepsilon}_d \cdot \vec{\varepsilon}_\gamma^* \times \vec{q}) N]. \quad (13)$$

The PC amplitude of  $nd \rightarrow {}^3H\gamma$  at the thermal energy is calculated and then used in the evaluation of the  $P_\gamma$  in sect.V.

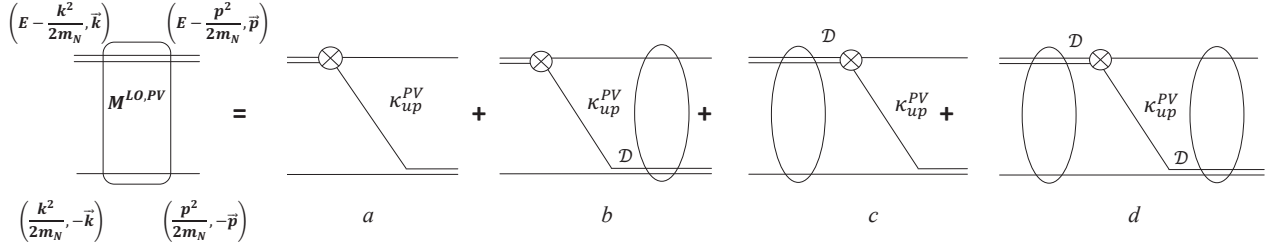


FIG. 3: The PV  $Nd$  scattering diagrams at LO. The dashed rectangular denotes the PV  $Nd$  scattering amplitude. Circle with a cross indicates the PV  $dNN$  vertex.  $\mathcal{K}_{up}^{PV}$  is the PV propagator of the exchanged nucleon when PV  $dNN$  vertex is in the upper side. Remaining notations are the same as fig.1. Time-reversed contributions not displayed.

### III. PARITY-VIOLATING SECTOR

#### A. Parity-violating $Nd$ scattering

The PV two-body transitions at the lowest order are  $^1S_0 \leftrightarrow ^3P_0$ ,  $^3S_1 \leftrightarrow ^1P_1$  and  $^3S_1 \leftrightarrow ^3P_1$ . The leading-order PV Lagrangian with dibaryon formalism is given by

$$\begin{aligned}
\mathcal{L}_{PV} = & - \left[ g^{(^3S_1-^1P_1)} d_t^{i\dagger} N^T i \left( \overleftarrow{\nabla} \sigma_2 \tau_2 - \sigma_2 \tau_2 \overrightarrow{\nabla} \right)_i N \right. \\
& + g_{(\Delta I=0)}^{(^1S_0-^3P_0)} d_s^{A\dagger} N^T i \left( \overleftarrow{\nabla} \sigma_2 \sigma_i \tau_2 \tau_A - \sigma_2 \sigma_i \tau_2 \tau_A \overrightarrow{\nabla} \right)_i N \\
& + g_{(\Delta I=1)}^{(^1S_0-^3P_0)} \epsilon^{3AB} d_s^{A\dagger} N^T i \left( \overleftarrow{\nabla} \sigma_2 \sigma_i \tau_2 \tau^B - \sigma_2 \sigma_i \tau_2 \tau^B \overrightarrow{\nabla} \right)_i N \\
& + g_{(\Delta I=2)}^{(^1S_0-^3P_0)} \mathcal{I}^{AB} d_s^{A\dagger} N^T i \left( \overleftarrow{\nabla} \sigma_2 \sigma_i \tau_2 \tau^B - \sigma_2 \sigma_i \tau_2 \tau^B \overrightarrow{\nabla} \right)_i N \\
& + g^{(^3S_1-^3P_1)} \epsilon^{ijk} d_t^{i\dagger} N^T \left( \overleftarrow{\nabla} \sigma_2 \sigma^k \tau_2 \tau_3 - \sigma_2 \sigma^k \tau_2 \tau_3 \overrightarrow{\nabla} \right)^j N \left. \right] \\
& + h.c. + \dots
\end{aligned} \tag{14}$$

In the above equation,  $g^{(\bar{X}-\bar{Y})}$  denotes the weak  $dNN$  coupling constant for the PV two-body transition between  $\bar{X}$  and  $\bar{Y}$  partial waves.  $\Delta I$  represents the isospin change in the PV vertex and  $\mathcal{I}=\text{diag}(1,1,-2)$  is a diagonal matrix in isospin space. The three-point in the last line represents all transitions that will be neglected at the very low energy.

For the three-nucleon systems, at the lowest order, there are four possible transitions

which mix S- and P-waves and conserve total angular momentum,

$$\begin{aligned}
{}^2S_{\frac{1}{2}} &\leftrightarrow {}^2P_{\frac{1}{2}} \quad , \quad {}^2S_{\frac{1}{2}} \leftrightarrow {}^4P_{\frac{1}{2}} \\
{}^4S_{\frac{3}{2}} &\leftrightarrow {}^2P_{\frac{3}{2}} \quad , \quad {}^4S_{\frac{3}{2}} \leftrightarrow {}^4P_{\frac{3}{2}} .
\end{aligned} \tag{15}$$

A systematic analysis by Griesshammer *et al.* [9] show that no parity-violating three-nucleon interaction (PV 3NI) is participated in the nucleon-deuteron system at the leading and next-to-leading orders in EFT( $\not{\pi}$ ). So, in the three-body systems, since all amplitudes converge at LO and NLO, no PV 3NI are needed for the renormalization. Thus, we use the Lagrangian in eq.(14) to obtain the LO PV  $Nd$  scattering amplitude for all possible channels in eq.(15).

The Feynman diagrams that contribute to the PV  $Nd$  scattering amplitude are shown in fig.3 [10]. In the cluster-configuration space, the contribution of these diagrams in fig.3 can be written after doing integration over energy and solid angle as

$$\begin{aligned}
t_{up}^{LO,PV}(X \rightarrow Y; E, k, p) &= 4\pi \mathcal{K}_{up}^{PV}(X \rightarrow Y; E, k, p) \\
&- \frac{2}{\pi} \int_0^\Lambda dq q^2 \left[ t^{LO,PC}(Y; E, q, p) \mathcal{D}^{LO}\left(E - \frac{q^2}{2m_N}, q\right) \mathcal{K}_{up}^{PV}(X \rightarrow Y; E, k, q) \right. \\
&\quad \left. + \mathcal{K}_{up}^{PV}(X \rightarrow Y; E, q, p) \mathcal{D}^{LO}\left(E - \frac{q^2}{2m_N}, q\right) t^{LO,PC}(X; E, k, q) \right] + \\
&+ \frac{1}{\pi^3} \int_0^\Lambda dq_1 q_1^2 \int_0^\Lambda dq_2 q_2^2 \left[ t^{LO,PC}(Y; E, q_2, p) \mathcal{D}^{LO}\left(E - \frac{q_2^2}{2m_N}, q_2\right) \right. \\
&\quad \left. \times \mathcal{K}_{up}^{PV}(X \rightarrow Y; E, q_1, q_2) \mathcal{D}^{LO}\left(E - \frac{q_1^2}{2m_N}, q_1\right) t^{LO,PC}(X; E, k, q_1) \right], \tag{16}
\end{aligned}$$

where  $t^{LO,PC}(X \text{ or } Y; E, k, p)$  is  $2 \times 2$  matrix for LO PC  $Nd$  scattering amplitudes, eqs.(7), (8), depending on the incoming (outgoing)  $X$  ( $Y$ ) partial wave.  $E = \frac{3k^2}{4m_N} - \frac{\vec{\gamma}_t^2}{m_N}$  and  $\vec{k}$  ( $\vec{p}$ ) are the center-of-mass energy and the incoming (outgoing) momentum, respectively. The PV kernel  $\mathcal{K}_{up}^{PV}(X \rightarrow Y; E, k, p)$  for all transitions with total angular momentum  $J = \frac{1}{2}$  is

given by [10] (see eq.(15) for all possible  $X \rightarrow Y$ )

$$\begin{aligned}
\mathcal{K}_{up}^{PV}(^2S_{\frac{1}{2}} \rightarrow ^2P_{\frac{1}{2}}; E, k, p) &= \frac{ym_N}{6\sqrt{2}\pi kp} [2pQ_0(-\varepsilon) + kQ_1(-\varepsilon)] \begin{pmatrix} \mathcal{S}_1 & -\mathcal{T} \\ \mathcal{S}_1 & -\mathcal{T} \end{pmatrix}, \\
\mathcal{K}_{up}^{PV}(^2P_{\frac{1}{2}} \rightarrow ^2S_{\frac{1}{2}}; E, k, p) &= \frac{ym_N}{6\sqrt{2}\pi kp} [2pQ_1(-\varepsilon) + kQ_0(-\varepsilon)] \begin{pmatrix} \mathcal{S}_1 & -\mathcal{T} \\ \mathcal{S}_1 & -\mathcal{T} \end{pmatrix}, \\
\mathcal{K}_{up}^{PV}(^2S_{\frac{1}{2}} \rightarrow ^4P_{\frac{1}{2}}; E, k, p) &= \frac{ym_N}{3\pi kp} [2pQ_0(-\varepsilon) + kQ_1(-\varepsilon)] \begin{pmatrix} \frac{\mathcal{S}_1 - \mathcal{S}_2}{3} & \mathcal{T} \\ 0 & 0 \end{pmatrix}, \\
\mathcal{K}_{up}^{PV}(^4P_{\frac{1}{2}} \rightarrow ^2S_{\frac{1}{2}}; E, k, p) &= \frac{ym_N}{6\pi kp} [2pQ_1(-\varepsilon) + kQ_0(-\varepsilon)] \begin{pmatrix} \mathcal{S}_2 & 0 \\ \mathcal{S}_2 & 0 \end{pmatrix}, \tag{17}
\end{aligned}$$

and with  $J = \frac{3}{2}$  by

$$\begin{aligned}
\mathcal{K}_{up}^{PV}(^4S_{\frac{3}{2}} \rightarrow ^2P_{\frac{3}{2}}; E, k, p) &= \frac{ym_N}{6\sqrt{2}\pi kp} [2pQ_0(-\varepsilon) + kQ_1(-\varepsilon)] \begin{pmatrix} \mathcal{S}_2 & 0 \\ \mathcal{S}_2 & 0 \end{pmatrix} Q_s^r, \\
\mathcal{K}_{up}^{PV}(^2P_{\frac{3}{2}} \rightarrow ^4S_{\frac{3}{2}}; E, k, p) &= \frac{ym_N}{3\sqrt{2}\pi kp} [2pQ_1(-\varepsilon) + kQ_0(-\varepsilon)] \begin{pmatrix} \frac{\mathcal{S}_1 - \mathcal{S}_2}{3} & \mathcal{T} \\ 0 & 0 \end{pmatrix} Q_s^r, \\
\mathcal{K}_{up}^{PV}(^4S_{\frac{3}{2}} \rightarrow ^4P_{\frac{3}{2}}; E, k, p) &= -\frac{\sqrt{10}ym_N}{6\pi kp} [2pQ_0(-\varepsilon) + kQ_1(-\varepsilon)] \begin{pmatrix} \frac{\mathcal{S}_1 - \mathcal{S}_2}{3} & 0 \\ 0 & 0 \end{pmatrix} Q_s^r, \\
\mathcal{K}_{up}^{PV}(^4P_{\frac{3}{2}} \rightarrow ^4P_{\frac{3}{2}}; E, k, p) &= -\frac{\sqrt{10}ym_N}{6\pi kp} [2pQ_1(-\varepsilon) + kQ_0(-\varepsilon)] \begin{pmatrix} \frac{\mathcal{S}_1 - \mathcal{S}_2}{3} & 0 \\ 0 & 0 \end{pmatrix} Q_s^r, \tag{18}
\end{aligned}$$

where  $\varepsilon = \frac{k^2 + p^2 - m_N E}{kp}$  and the  $(Q_s^r)_\beta^\alpha = \delta_s^r \delta_\beta^\alpha - \frac{1}{3}(\sigma^r \sigma_s)_\beta^\alpha$  is the spin quartet projector. The index  $\alpha$  ( $\beta$ ) denotes the spin of the outgoing (incoming) nucleon and  $r$  ( $s$ ) is the spin component of the outgoing (incoming)  $^3S_1$  dibaryon.  $Q_L(z)$  is the  $L$ -th Legendre polynomials of the second kind with the complex argument. The "up" subscript represents the PV vertex in the upper side of the diagrams. The  $\mathcal{S}_1$ ,  $\mathcal{S}_2$  and  $\mathcal{T}$  are independent linear combinations of the PV coupling constants,  $g^{(\bar{X}-\bar{Y})}$ ,

$$\begin{aligned}
\mathcal{S}_1 &= 3g^{(^3S_1-^1P_1)} + 2\tau_3 g^{(^3S_1-^3P_1)}, \\
\mathcal{S}_2 &= 3g^{(^3S_1-^1P_1)} - \tau_3 g^{(^3S_1-^3P_1)}, \\
\mathcal{T} &= 3g_{(\Delta I=0)}^{(^1S_0-^3P_0)} + 2\tau_3 g_{(\Delta I=1)}^{(^1S_0-^3P_0)}, \tag{19}
\end{aligned}$$

where the value of the  $\tau_3$  is +1 and -1 for the scattering on the proton and neutron, respectively.

We note that the eq.(16) is not a Faddeev equation. However the Faddeev equations in the eqs.(7), (8) should be solved numerically for the PC  $Nd$  scattering amplitude and then replace the results in eq.(16). We solve eq.(16) numerically.

The calculation of the time-reversed contributions of the diagrams in fig.3 is the same as explained above. We must only substitute the  $\mathcal{K}_{down}^{PV}(X \rightarrow Y; E, k, p)$  in eq.(16) with  $\mathcal{K}_{up}^{PV}(X \rightarrow Y; E, k, p)$  to obtain the time-reversed contribution of the diagrams in fig.3. The  $\mathcal{K}_{down}^{PV}(X \rightarrow Y; E, k, p)$  can be written as

$$\mathcal{K}_{down}^{PV}(X \rightarrow Y; E, k, p)_{s\beta}^{r\alpha} = \left[ \mathcal{K}_{up}^{PV}(Y \rightarrow X; E, p, k)_{r\alpha}^{s\beta} \right]^\dagger. \quad (20)$$

Finally, after multiplication of the wave function normalization factor the physical amplitude of the neutron-deuteron scattering in the on-shell point ( $k = p$ ) is

$$T^{LO,PV}(X \rightarrow Y; E, k, k) = \begin{pmatrix} \sqrt{\mathcal{Z}_{LO}} & 0 \end{pmatrix} t^{LO,PV}(X \rightarrow Y; E, k, k) \begin{pmatrix} \sqrt{\mathcal{Z}_{LO}} \\ 0 \end{pmatrix}, \quad (21)$$

where  $t^{LO,PV}$  is the sum of both  $t_{up}^{LO,PV}$  and  $t_{down}^{LO,PV}$  and  $\mathcal{Z}_{LO} = \frac{2\gamma t}{m_N}$  is the LO deuteron wave function normalization factor in Z-parametrization.

## B. Parity-violating $nd \rightarrow {}^3H\gamma$ system

In this section, we concentrate on the PV amplitude of  $nd \rightarrow {}^3H\gamma$  process. For this purpose, we need to obtain the electromagnetic (EM) matrix elements that contribute at the thermal energy ( $2.5 \times 10^{-8} \text{MeV}$ ) near threshold. In the low-energy regime, we work with the Lagrangian introduced in eq.(14) for the PV interaction.

At threshold, E1 transition contributes a dominate part in the PV neutron-deuteron radiative capture process. Obviously, as we move above the threshold we must also add the parity-violating M1 transition to the leading E1 amplitude. In the present calculations, we introduce the diagrams that contribute to the E1 PV neutron-deuteron radiative capture process. These diagrams are shown schematically in figs.4 and 5. We identify the diagrams in fig.4 as the set (I) and those of fig.5 as the set (II). The dashed rectangular with dashed line around it in fig.4 denotes the PV  $Nd$  scattering amplitude corresponding to the diagrams

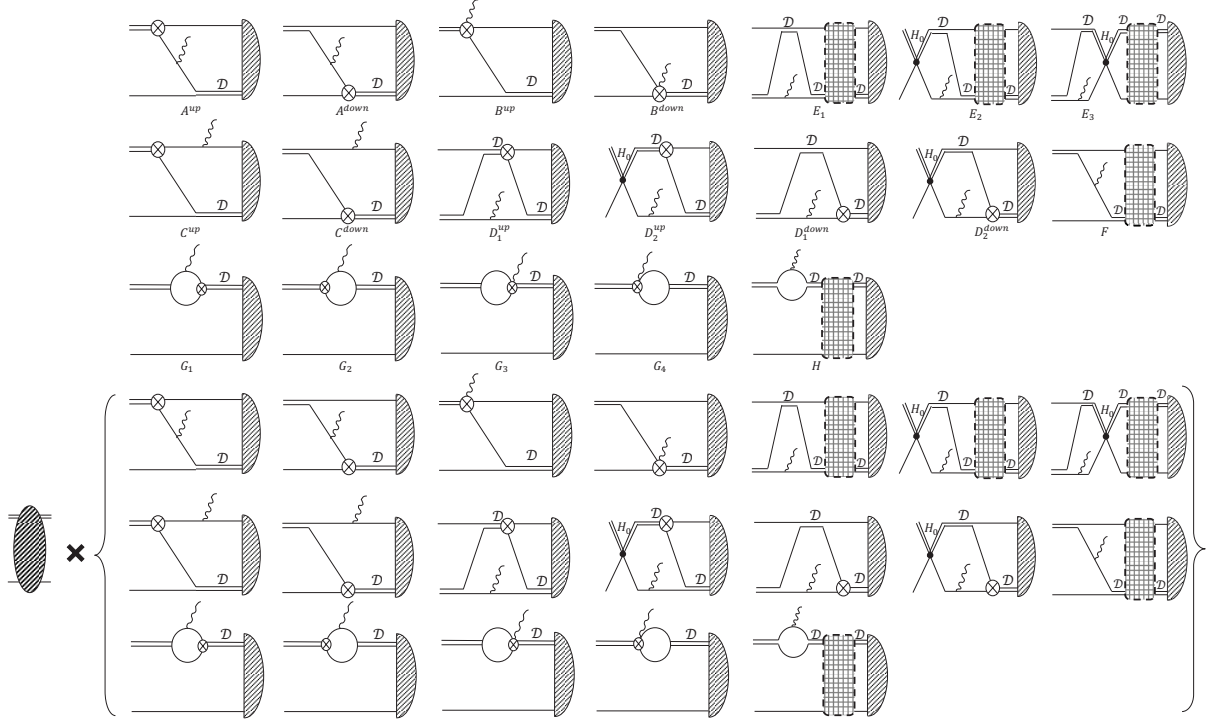


FIG. 4: The set (I) diagrams of the PV  $nd \rightarrow {}^3H\gamma$  process at LO. Circle with a cross and wavy line is the PV  $\gamma dNN$  vertex. The dashed rectangular with dashed line around it denotes the PV  $Nd$  scattering amplitude depicted in fig.3 without participation of the diagrams which have the full PC  $Nd$  scattering in the right hand side.  $H_0$  is the three-body force which has been introduced in fig.1. All notations are the same as the previous figures.

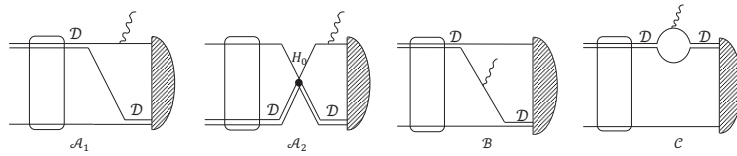


FIG. 5: The set (II) diagrams of the PV  $nd \rightarrow {}^3H\gamma$  process at LO. The dashed rectangular with solid line around it is the PV  $Nd$  scattering amplitude shown in fig.3. All notation are the same as the previous figures.

$a$ ,  $c$  and time-reversed contribution of  $a$ ,  $b$  shown in fig.3. The dashed rectangular with solid line around it in fig.5 is the PV  $Nd$  scattering amplitude depicted in fig.3. In figs.4 and 5 dashed oval and dashed half-oval are the same as before.

We consider only the one-body current for E1 interaction and we employ the "convection" nucleon current for the photon-nucleon-nucleon ( $\gamma NN$ ) vertex that can be written generally

by [17]

$$J_N(\vec{r}) = \frac{1}{2} \sum_j (1 + \tau_3^{(j)}) \left[ \frac{\vec{P}}{2m_N} \delta(\vec{r} - \vec{r}_j) + \delta(\vec{r} - \vec{r}_j) \frac{\vec{P}'}{2m_N} \right] \cdot \vec{\varepsilon}_\gamma^*, \quad (22)$$

where  $\vec{P}$  and  $\vec{P}'$  are momenta for the incoming and outgoing nucleons.  $\tau_3^{(j)}$  and  $\vec{r}_j$  are the 3<sup>rd</sup>-component of the isospin operator and the position of the  $j^{\text{th}}$ -nucleon, respectively. For the single nucleon, it is reduced to

$$\frac{1}{2m_N} (1 + \tau_3) \frac{1}{2} (\vec{P} + \vec{P}') \cdot \vec{\varepsilon}_\gamma^*. \quad (23)$$

The PV photon-dibaryon-nucleon-nucleon ( $\gamma dNN$ ) vertex in fig.4 is given by the minimal substitution of  $\vec{\nabla} \rightarrow \vec{\nabla} + ie \frac{1+\tau_3}{2} \vec{A}$  in the Lagrangian of eq.(14) with  $\vec{A}$  as an external field.

We have both E1 and PV interactions together, so it is obvious that the neutron-deuteron system can change from the initial channel  ${}^2S_{\frac{1}{2}}$  or  ${}^4S_{\frac{3}{2}}$  to the final channel  ${}^2S_{\frac{1}{2}}$  or  ${}^4S_{\frac{3}{2}}$  at the thermal energy. Thus, there are four possible transitions,

$$\begin{aligned} {}^2S_{\frac{1}{2}} &\rightarrow {}^2S_{\frac{1}{2}}, & {}^2S_{\frac{1}{2}} &\rightarrow {}^4S_{\frac{3}{2}}, \\ {}^4S_{\frac{3}{2}} &\rightarrow {}^2S_{\frac{1}{2}}, & {}^4S_{\frac{3}{2}} &\rightarrow {}^4S_{\frac{3}{2}}, \end{aligned} \quad (24)$$

where the first and third transitions can make  ${}^3H$  and  ${}^3He$ . So, we have two E1 transitions for the PV neutron radiative capture by deuteron, corresponding to the  $X$  partial wave of the incoming neutron-deuteron system ( $X = {}^2S_{\frac{1}{2}}$  and  $X = {}^4S_{\frac{3}{2}}$ ).

The spin structure of the E1 matrix element of PV  $nd \rightarrow {}^3H\gamma$  process can be written as

$$i(t^\dagger \sigma_a N) (\vec{\varepsilon}_d \times \vec{\varepsilon}_\gamma^*)_a, \quad (t^\dagger N) (\vec{\varepsilon}_d \cdot \vec{\varepsilon}_\gamma^*). \quad (25)$$

We can obtain for both incoming doublet ( $X = {}^2S_{\frac{1}{2}}$ ) and quartet ( $X = {}^4S_{\frac{3}{2}}$ ) channels

$$\begin{aligned} \mathcal{W}^{PV}({}^2S_{\frac{1}{2}}) &[ t^\dagger (\vec{\varepsilon}_d \cdot \vec{\varepsilon}_\gamma^* + i\vec{\sigma} \cdot \vec{\varepsilon}_d \times \vec{\varepsilon}_\gamma^*) N ], \\ \mathcal{W}^{PV}({}^4S_{\frac{3}{2}}) &[ t^\dagger (\vec{\varepsilon}_d \cdot \vec{\varepsilon}_\gamma^* + i\vec{\sigma} \cdot \vec{\varepsilon}_d \times \vec{\varepsilon}_\gamma^*) N ]. \end{aligned}$$

where  $\mathcal{W}^{PV}(X)$  is the amplitude of the E1 transition for the incoming  $X$  partial wave. In this section, we are going to calculate  $\mathcal{W}^{PV}(X)$  from all possible Feynman diagrams introduced in figs.4 and 5 for the PV  $nd \rightarrow {}^3H\gamma$  process.

If we want to use the PV  $Nd$  scattering amplitude for the calculation of some diagrams in the set (I) and also the set (II), we should make clear the possible incoming and outgoing partial waves for PV  $Nd$  scattering amplitude.

For the  $\mathcal{A}_1$ ,  $\mathcal{A}_2$ ,  $\mathcal{B}$  and  $\mathcal{C}$  diagrams in fig.5, we can schematically represent the PV and E1 transitions as

$$X \xrightarrow{PV} Y \xrightarrow{E1} {}^2S_{\frac{1}{2}} (\text{triton}), \quad (26)$$

where above scheme shows the incoming and outgoing partial wave of the PV  $Nd$  scattering are  $X$  and  $Y$ , respectively. At the thermal energy,  $X$  can be  ${}^2S_{\frac{1}{2}}$  and  ${}^4S_{\frac{3}{2}}$ , as incoming doublet and quartet channels, and  $Y$  also can be  ${}^2P_{\frac{1}{2}}$ ,  ${}^2P_{\frac{3}{2}}$ ,  ${}^4P_{\frac{1}{2}}$  or  ${}^4P_{\frac{3}{2}}$  (see eq.(15)). Furthermore, because the electric interaction does not change the relative spin of the particles, all E1 transitions which can create the triton are

$${}^2P_{\frac{1}{2}} \xrightarrow{E1} {}^2S_{\frac{1}{2}}, \quad {}^2P_{\frac{3}{2}} \xrightarrow{E1} {}^2S_{\frac{1}{2}}. \quad (27)$$

So, from eqs.(15), (26) and (27), we finally have only two possible transitions

$$\begin{aligned} {}^2S_{\frac{1}{2}} &\xrightarrow{PV} {}^2P_{\frac{1}{2}} \xrightarrow{E1} {}^2S_{\frac{1}{2}}, \\ {}^4S_{\frac{3}{2}} &\xrightarrow{PV} {}^2P_{\frac{3}{2}} \xrightarrow{E1} {}^2S_{\frac{1}{2}}, \end{aligned} \quad (28)$$

from the initial S-wave state to triton for the  $\mathcal{A}_1$ ,  $\mathcal{A}_2$ ,  $\mathcal{B}$  and  $\mathcal{C}$  diagrams which are shown in fig.5. Hence,  $t^{LO,PV}({}^2S_{\frac{1}{2}} \rightarrow {}^2P_{\frac{1}{2}})$  and  $t^{LO,PV}({}^4S_{\frac{3}{2}} \rightarrow {}^2P_{\frac{3}{2}})$  amplitudes are needed for calculating the contribution of these diagrams.

A similar arguments can be expressed for the  $E_j$  ( $j = 1, 2, 3$ ),  $F$  and  $H$  diagrams in the set (I). Consequently, for these diagrams, one can see that there are two possible transitions which are presented schematically as

$$\begin{aligned} {}^2S_{\frac{1}{2}} &\xrightarrow{E1} {}^2P_{\frac{1}{2}} \xrightarrow{PV} {}^2S_{\frac{1}{2}}, \\ {}^4S_{\frac{3}{2}} &\xrightarrow{E1} {}^4P_{\frac{1}{2}} \xrightarrow{PV} {}^2S_{\frac{1}{2}}. \end{aligned} \quad (29)$$

Thus, for these diagrams, we require  $\tilde{t}^{LO,PV}({}^2P_{\frac{1}{2}} \rightarrow {}^2S_{\frac{1}{2}})$  and  $\tilde{t}^{LO,PV}({}^4P_{\frac{1}{2}} \rightarrow {}^2S_{\frac{1}{2}})$  amplitudes to obtain the contribution of  $E_j$ ,  $F$  and  $H$  diagrams in fig.4.  $\tilde{t}^{LO,PV}$  denotes the PV  $Nd$  scattering amplitude corresponding to the diagrams  $a$ ,  $c$  and time-reversed contribution of  $a$ ,  $b$  shown in fig.3.

Now, one can be able to begin the calculation of the sets (I) and (II) diagrams. Initially, we describe the set (I) (fig.4) and then proceed to explain the set (II) (fig.5). Let us consider the PV LECs in eq.(14) and rename them conveniently from up to down by  $g_1$  to  $g_5$ , respectively; for example,  $g_2$  is  $g_{\Delta I=0}^{(1S_0-3P_0)}$ .

The amplitude of all diagrams in fig.4, for the incoming X channel, can be written as

$$W_I^{PV}(X; E_i, E_f, k) = S(X; E_i, E_f, k) - \frac{1}{2\pi^2} \int q^2 dq S(X; E_i, E_f, q) \mathcal{D}^{LO}(E_i - \frac{q^2}{2m_N}, q) t^{LO,PC}(X; E_i, k, q), \quad (30)$$

where subscript "I" in  $W_I^{PV}$  represents the contribution of the set (I) diagrams and  $X$  is the partial wave of the incoming channel (doublet or quartet). We assume  $E_i = E = \frac{3}{4} \frac{k^2}{m_N} - \frac{\gamma_t^2}{m_N}$  and  $E_f = -B_t$ .

In the above equation,  $S(X; E_i, E_f, k)$  kernel is given by

$$S(X; E_i, E_f, k) = S_1(X; E_i, E_f, k) + S_2(X; E_i, E_f, k) + S_3(X; E_i, E_f, k), \quad (31)$$

where  $S_i$  ( $i = 1, 2, 3$ ) is the contribution of all diagrams in the  $i$ -th line of fig.4. The results of the  $S_1$  and  $S_2$  kernels for two incoming doublet and quartet channels are presented in Appendix B, however we introduce the  $S_3$  kernel in the following. We note that the groups of the diagrams represented by  $C$ ,  $D$  and  $E$  in fig.4 have two contributions corresponding to the poles in the nucleon propagators before and after the photon creation.

The contribution of all diagrams in the line 3 of fig.4, for the incoming  $X$  channel, in the cluster-configuration space is given by

$$S_3(X; E_i, E_f, k) = t^{3H^\dagger}(k) \mathcal{D}^{LO}(E_f - \frac{k^2}{2m_N}, k) O(X; E_i, E_f, k) + - \frac{1}{2\pi^2} \int q'^2 dq' t^{3H^\dagger}(q') \mathcal{D}^{LO}(E_f - \frac{q'^2}{2m_N}, q') \times \times \tilde{t}^{LO,PV}(Y \rightarrow {}^2S_{\frac{1}{2}}; E_f, k, q') \times \times \mathcal{D}^{LO}(E_f - \frac{k^2}{2m_N}, k) \tilde{O}(X \rightarrow Y; E_i, E_f, k), \quad (32)$$

where, as previously explained in eq.29,  $Y$  partial wave should be  ${}^2P_{\frac{1}{2}}$  and  ${}^4P_{\frac{1}{2}}$  for  $X = {}^2S_{\frac{1}{2}}$  and  ${}^4S_{\frac{3}{2}}$ , respectively. So, we evaluate for the corresponding partial waves the following  $O$

matrices,

$$\begin{aligned}
O(^2S_{\frac{1}{2}}; E_i, E_f, q) = & \\
& -\frac{eym_N}{18\sqrt{2}\pi} \left\{ 3 \left[ \sqrt{\frac{3q^2}{4} - m_N E_f} \begin{pmatrix} -2g_5 & \tau_3 g_2 \\ \tau_3 g_1 & 0 \end{pmatrix} + \sqrt{\frac{3q^2}{4} - m_N E_i} \begin{pmatrix} -2g_5 & \tau_3 g_1 \\ \tau_3 g_2 & 0 \end{pmatrix} \right] \right. \\
& \left. + G(E_i, E_f, q) \begin{pmatrix} 4g_5 & -\tau_3(g_1 + g_2) \\ -\tau_3(g_1 + g_2) & 0 \end{pmatrix} \right\}, \\
O(^4S_{\frac{3}{2}}; E_i, E_f, q) = & \\
& -\frac{eym_N}{9\sqrt{6}\pi} \left\{ 3 \left[ \sqrt{\frac{3q^2}{4} - m_N E_f} \begin{pmatrix} g_5 & 0 \\ \tau_3 g_1 & 0 \end{pmatrix} + \sqrt{\frac{3q^2}{4} - m_N E_i} \begin{pmatrix} g_5 & 0 \\ \tau_3 g_2 & 0 \end{pmatrix} \right] \right. \\
& \left. + G(E_i, E_f, q) \begin{pmatrix} -2g_5 & 0 \\ -\tau_3(g_1 + g_2) & 0 \end{pmatrix} \right\}. \tag{33}
\end{aligned}$$

The calculated  $\tilde{O}(X \rightarrow Y)$  matrix in eq.(32) is given for the required partial waves by

$$\begin{aligned}
\tilde{O}(^2S_{\frac{1}{2}} \rightarrow ^2P_{\frac{1}{2}}; E_i, E_f, q) &= -\frac{ey^2}{96\pi} \frac{q}{E_f - E_i} \left[ \sqrt{\frac{3q^2}{4} - m_N E_i} - \sqrt{\frac{3q^2}{4} - m_N E_f} \right] \begin{pmatrix} 1 & 0 \\ 0 & 1 \end{pmatrix}, \\
\tilde{O}(^4S_{\frac{3}{2}} \rightarrow ^4P_{\frac{1}{2}}; E_i, E_f, q) &= \sqrt{\frac{2}{3}} \tilde{O}(^2S_{\frac{1}{2}} \rightarrow ^2P_{\frac{1}{2}}; E_i, E_f, q) \begin{pmatrix} 1 & 0 \\ 0 & 0 \end{pmatrix}, \\
\tilde{O}(^2P_{\frac{1}{2}} \rightarrow ^2S_{\frac{1}{2}}; E_i, E_f, q) &= \tilde{O}(^2S_{\frac{1}{2}} \rightarrow ^2P_{\frac{1}{2}}; E_i, E_f, q), \\
\tilde{O}(^2P_{\frac{3}{2}} \rightarrow ^2S_{\frac{1}{2}}; E_i, E_f, q) &= \frac{2}{\sqrt{3}} \tilde{O}(^2S_{\frac{1}{2}} \rightarrow ^2P_{\frac{1}{2}}; E_i, E_f, q). \tag{34}
\end{aligned}$$

We have also presented the results of  $\tilde{O}(^2P_{\frac{1}{2}} \rightarrow ^2S_{\frac{1}{2}})$  and  $\tilde{O}(^2P_{\frac{3}{2}} \rightarrow ^2S_{\frac{1}{2}})$  in eq.(34) because they are required in the following calculation regarding the diagram  $\mathcal{C}$  in fig.5. In eq.(33) the  $G$  function is

$$\begin{aligned}
G(E_i, E_f, q) = & \frac{1}{m_N(E_f - E_i)} \left\{ \frac{3q^2}{4} \left[ \left( \frac{3q^2}{4} - m_N E_i \right)^{1/2} - \left( \frac{3q^2}{4} - m_N E_f \right)^{1/2} \right] \right. \\
& \left. - \left[ \left( \frac{3q^2}{4} - m_N E_i \right)^{3/2} - \left( \frac{3q^2}{4} - m_N E_f \right)^{3/2} \right] \right\}. \tag{35}
\end{aligned}$$

The above results are evaluated by considering the suitable partial-wave projections for the incoming and outgoing channels. One can see all projection operators in the cluster-configuration space which are used in our calculations in the ref.[10].

All other possible diagrams in the calculation of PV  $nd \rightarrow {}^3H\gamma$  amplitude, at the thermal energy, are shown in fig.5 as the set (II).

We note that the  $\mathcal{A}_2$  diagram in fig.5 has no contribution in  $\mathcal{W}^{PV}$  because the three-body force introduced in sect.IIA is zero for the P-wave ( $L = 1$ ). The contribution of the  $\mathcal{A}_1$  and  $\mathcal{B}$  diagrams in fig.5, for two incoming doublet ( $X = {}^2S_{\frac{1}{2}}$ ) and quartet ( $X = {}^4S_{\frac{3}{2}}$ ) channels is given by

$$W_{II}^{PV\mathcal{A}_1+\mathcal{B}}(X; E_i, E_f, k) = -\frac{1}{2\pi^2} \int q^2 dq [\mathcal{A}_1(Y; E_i, E_f, q) + \mathcal{B}(Y; E_i, E_f, q)] \times \\ \times \mathcal{D}^{LO}(E_i - \frac{q^2}{2m_N}, q) t^{LO,PV}(X \rightarrow Y; E_i, k, q), \quad (36)$$

where  $\mathcal{A}_1$  and  $\mathcal{B}$  can be written as

$$\mathcal{A}_1(Y; E_i, E_f, q) = a_Y \frac{ey^2}{E_f - E_i} \int \frac{d^3q'}{(2\pi)^3} \frac{1}{q} t^{3H^\dagger}(q') \times \\ \times \left[ \mathcal{D}^{LO}(E_i - \frac{q'^2}{2m_N}, q') \frac{\vec{q} \cdot \vec{q}'}{m_N E_i - q^2 - q'^2 - \vec{q} \cdot \vec{q}'} \right. \\ \left. - \mathcal{D}^{LO}(E_f - \frac{q'^2}{2m_N}, q') \frac{\vec{q} \cdot \vec{q}'}{m_N E_f - q^2 - q'^2 - \vec{q} \cdot \vec{q}'} \right] \\ \times \begin{pmatrix} -3(1 + \tau_3) & 9(1 + \tau_3) \\ 3(3 - \tau_3) & -(3 - \tau_3) \end{pmatrix}, \quad (37)$$

and

$$\mathcal{B}(Y; E_i, E_f, q) = a_Y \frac{ey^2}{E_f - E_i} \frac{1}{q} \int \frac{d^3q'}{(2\pi)^3} t^{3H^\dagger}(q') \times \\ \times \mathcal{D}^{LO}(E_f - \frac{q'^2}{2m_N}, q') \left[ \frac{\vec{q} \cdot (\vec{q} + \vec{q}')}{m_N E_i - q^2 - q'^2 - \vec{q} \cdot \vec{q}'} \right. \\ \left. - \frac{\vec{q} \cdot (\vec{q} + \vec{q}')}{m_N E_f - q^2 - q'^2 - \vec{q} \cdot \vec{q}'} \right] \begin{pmatrix} -3(1 - \tau_3) & 3(3 + \tau_3) \\ 3(3 + \tau_3) & -(3 + 5\tau_3) \end{pmatrix}. \quad (38)$$

In the above equations,  $a_Y$  is  $\frac{1}{96}$  for  $Y = {}^2P_{\frac{1}{2}}$  and  $\frac{1}{32\sqrt{3}}$  for  $Y = {}^2P_{\frac{3}{2}}$  partial wave.

The final diagram in the  $P_\gamma$  calculation is the  $\mathcal{C}$  diagram shown in fig.5. After applying the Feynman rules and the appropriate incoming and outgoing projections, one can see that

the contribution of the  $\mathcal{C}$  diagram is given by

$$\begin{aligned}
W_{II}^{PV\mathcal{C}}(X; E_i, E_f, k) = & -\frac{1}{2\pi^2} \int q^2 dq t^{3H^\dagger}(q) \times \\
& \times \mathcal{D}^{LO}(E_f - \frac{q^2}{2m_N}, q) \tilde{O}(Y \rightarrow {}^2S_{\frac{1}{2}}; E_i, E_f, q) \\
& \times \mathcal{D}^{LO}(E_i - \frac{q^2}{2m_N}, q) t^{LO,PV}(X \rightarrow Y; E_i, k, q). \tag{39}
\end{aligned}$$

In the eqs.(36)-(39),  $Y$  partial wave as explained in eq.29 is  ${}^2P_{\frac{1}{2}}$  and  ${}^2P_{\frac{3}{2}}$  for the incoming doublet and quartet channels, respectively. The calculated results of the  $\tilde{O}({}^2P_{\frac{1}{2}} \rightarrow {}^2S_{\frac{1}{2}})$  and  $\tilde{O}({}^2P_{\frac{3}{2}} \rightarrow {}^2S_{\frac{1}{2}})$  are previously introduced in eq.(34).

We emphasize that the diagrams for the interaction of  $H_0$  with a photon has no contribution because  $H_0$  has no derivatives, so it is not affected by the minimal substitution  $\vec{P} \rightarrow \vec{P} + e\vec{A}$ .

Finally, the physical amplitude of all diagrams in the sets (I) and (II) is given by

$$\mathcal{W}^{PV}(X; E_i, k) = \left( W_I^{PV}(X; E_i, k) + W_{II}^{PV}(X; E_i, k) \right) \begin{pmatrix} \sqrt{\mathcal{Z}_{LO}} \\ 0 \end{pmatrix}, \tag{40}$$

where  $W_I^{PV}$  and  $W_{II}^{PV}$  are the amplitudes of all diagrams in the set (I) and (II), respectively. We note that the value of  $\tau_3$  is -1 for  $nd \rightarrow {}^3H\gamma$  as previously explained in the sect.III A.

#### IV. NUMERICAL CALCULATION

In the calculation of the photon circular polarization,  $P_\gamma$ , in  $nd \rightarrow {}^3H\gamma$  process we need to evaluate the total amplitude of this process. The total amplitude is sum of both PC and PV contributions that introduced in the previous sections. We generally classify the numerical computation in three steps.

In the first step, we compute the full-offshell doublet and quartet PC neutron-deuteron scattering amplitudes and the triton wave function at LO. The PC neutron-deuteron scattering and the triton wave function are used in the calculations of the PC and PV  $nd \rightarrow {}^3H\gamma$  amplitudes. The PC neutron-deuteron scattering is obtained by solving numerically the Faddeev equations in eqs.(7) and (8). We solve it by the Hetherington-Schick method [18–20] in a mathematica code with an arbitrary cutoff momentum  $\Lambda$ , for detail see ref.[15]. We also obtain the triton wave function by solving eq.(11) as previously explained.

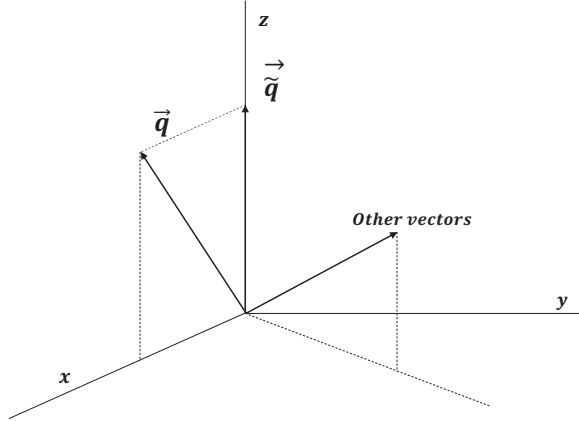


FIG. 6: Coordinate system used in the integration over solid angles.

In the second step, we use the off-shell PC neutron-deuteron scattering amplitude which is computed numerically in the previous step in order to obtain the PV neutron-deuteron scattering amplitude of the diagrams in fig.3. We have written a new mathematica code for this step and use the results of the PC neutron-deuteron scattering amplitude as input data. Note that we choose the same cutoff momentum  $\Lambda$  for the PC neutron-deuteron scattering and the PV sector calculations.

The final step is the calculation of the PC (M1) and PV (E1)  $nd \rightarrow {}^3H\gamma$  amplitudes. The PC amplitude of  $nd \rightarrow {}^3H\gamma$  process is obtained by using the PC neutron-deuteron scattering amplitude and the triton wave function results.

For the calculation of the PV amplitude we require to evaluate the set (I) diagrams of PV  $nd \rightarrow {}^3H\gamma$ , fig.4. Therefore, we must compute the  $S(X; E_i, E_f, q)$  kernel which is introduced in eq.(31) (the contribution of the diagrams in the lines 1, 2 and 3 of set (I)). For the diagrams in the Lines 4, 5 and 6 of the set (I), we add the half-offshell PC neutron-deuteron scattering amplitude from the left side to the  $S(X; E_i, E_f, q)$  kernel (see eq.(30)).

Finally, the set (II) diagrams in fig.5 also computed similar to the set (I) diagrams by using the appropriate half-offshell PV neutron-deuteron scattering and the triton wave function data. We solve the integrations numerically by using the gaussian quadrature weights and the same cutoff  $\Lambda$  as before.

We emphasize that for integration over the solid angle, we choose a coordinate system in which the momentum of outgoing photon is in the z direction and the  $q$  momentum is in the x-z plane (see fig.6).

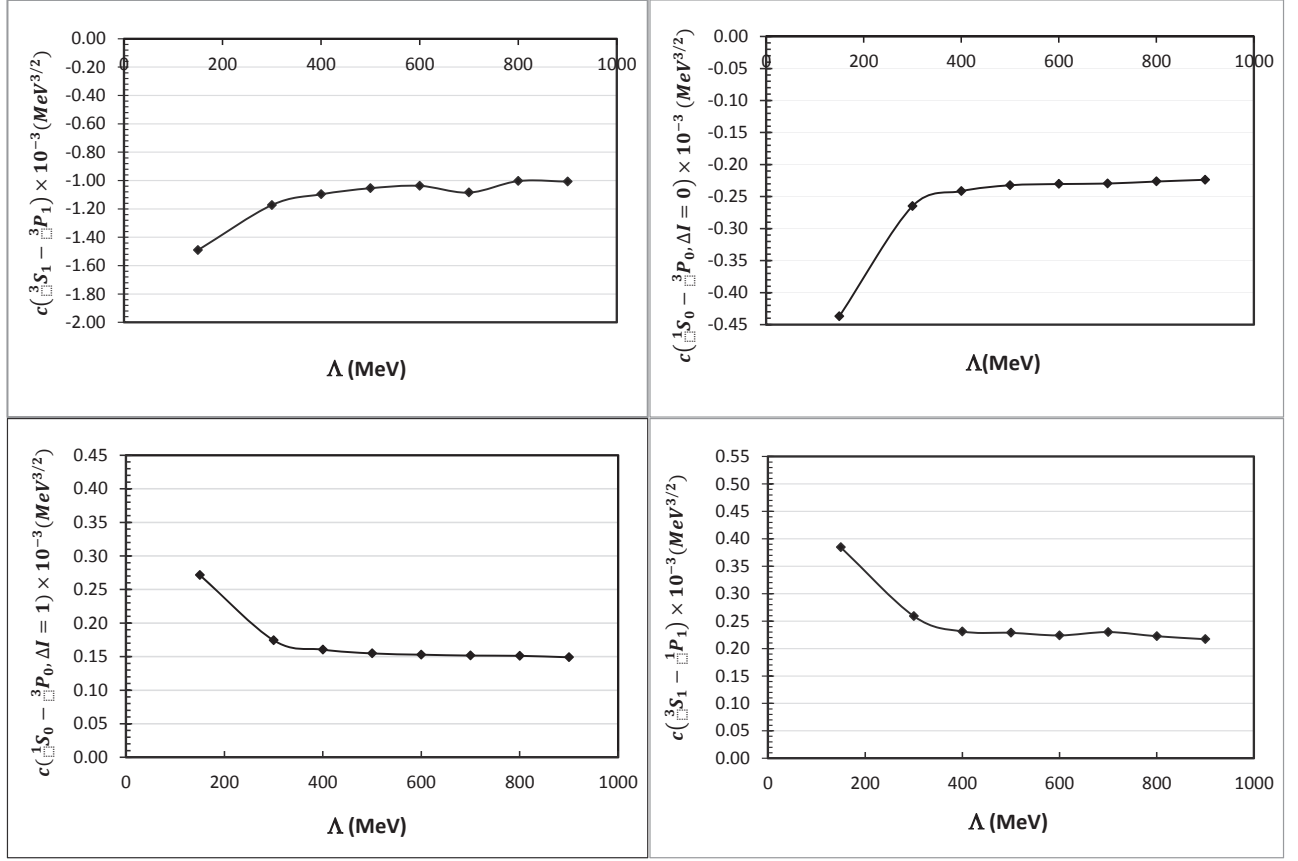


FIG. 7: Variation of the  $c(\bar{X} - \bar{Y})$  with cutoff momentum at thermal energy ( $2.5 \times 10^{-8}$  MeV).

## V. RESULTS

In this work, we have concentrated on the evaluation of photon circular polarization,  $P_\gamma$ , in  $nd \rightarrow {}^3H\gamma$  process and obtaining a new relation, which is useful for extracting five leading independent LECs.

The PV polarization of photon is given by

$$P_\gamma = \frac{\sigma_+ - \sigma_-}{\sigma_+ + \sigma_-}, \quad (41)$$

where  $\sigma_+$  and  $\sigma_-$  are the cross section for the photons with right and left helicity, respectively.

We know that the cross sections are calculated with spin summation on the square amplitude. Therefore one can conclude that the PV polarization of photon can be written

as

$$P_\gamma = 2 \frac{\text{Re} \left[ \mathcal{W}^{PC\dagger}(^2S_{\frac{1}{2}}) \mathcal{W}^{PV}(^2S_{\frac{1}{2}}) + \mathcal{W}^{PC\dagger}(^4S_{\frac{3}{2}}) \mathcal{W}^{PV}(^4S_{\frac{3}{2}}) \right]}{|\mathcal{W}^{PC}(^2S_{\frac{1}{2}})|^2 + |\mathcal{W}^{PC}(^4S_{\frac{3}{2}})|^2}, \quad (42)$$

where  $\mathcal{W}^{PC}(X)$  and  $\mathcal{W}^{PV}(X)$  are the PC and PV amplitudes of  $nd \rightarrow ^3H\gamma$  process which are introduced and evaluated in sects.II B and III B, respectively.

From eq.(42), one can evaluate the  $P_\gamma$  in terms of the PV LECs. So, for the photon circular polarization, we have

$$\begin{aligned} P_\gamma = & c(^3S_1 - ^1P_1) g(^3S_1 - ^1P_1) \\ & + c(^1S_0 - ^3P_0, \Delta I = 0) g_{(\Delta I=0)}(^1S_0 - ^3P_0) \\ & + c(^1S_0 - ^3P_0, \Delta I = 1) g_{(\Delta I=1)}(^1S_0 - ^3P_0) \\ & + c(^3S_1 - ^3P_1) g(^3S_1 - ^3P_1), \end{aligned} \quad (43)$$

where  $c(\bar{X} - \bar{Y})$  is calculated numerically and shown in fig.7. The  $P_\gamma$  does not contain  $g_{(\Delta I=2)}(^1S_0 - ^3P_0)$  term because the  $Nd$  system is an iso-doublet and PV coupling  $g_{(\Delta I=2)}(^1S_0 - ^3P_0)$  cannot contribute.

According to the table I which is shown below, we have calculated the  $Abs[1 - \frac{c(\bar{X}-\bar{Y}) \text{ at } \Lambda=400 \text{ MeV}}{c(\bar{X}-\bar{Y}) \text{ at } \Lambda=900 \text{ MeV}}]$  for the different incoming and outgoing partial waves. These results

TABLE I: Results of the cutoff variation of  $c(\bar{X} - \bar{Y})$ , for the different incoming and outgoing partial waves, between  $\Lambda = 400$  MeV and  $\Lambda = 900$  MeV.

$c(\bar{X} - \bar{Y})$	$Abs[1 - \frac{c(\bar{X}-\bar{Y}) \text{ at } \Lambda=400 \text{ MeV}}{c(\bar{X}-\bar{Y}) \text{ at } \Lambda=900 \text{ MeV}}]$
$c(^3S_1 - ^1P_1)$	0.0648
$c(^1S_0 - ^3P_0, \Delta I = 0)$	0.0797
$c(^1S_0 - ^3P_0, \Delta I = 1)$	0.0768
$c(^3S_1 - ^3P_1)$	0.0891

indicate that the cutoff dependence is less than 0.10. This small variation can be removed with the consideration of the higher order corrections.

Therefore, the variation of the  $c(\bar{X} - \bar{Y})$  indicates the ignorable dependence on cutoff at the leading order. So, it can be concluded that at LO for PV neutron radiative capture by deuteron no new three-nucleon interaction is needed.

In the numerical calculation for the results shown in 7, we used for the nucleon mass  $m_N = 938.918$  MeV, deuteron binding momentum  $\gamma_t = 45.7025$  MeV, effective range of deuteron  $\rho_d = 1.764$  fm, effective range of  $NN$  singlet channel  $r_0 = 2.73$  fm, scattering length in singlet channel of  $-23.714$  fm and a triton binding energy  $B_t = 8.48$  MeV.

It is obvious that the PV coupling constants are not predicted by the EFT but can be estimated on dimensional grounds. We expect that the magnitude of the PV coupling to be of the order [10]

$$|g^{(\bar{X}-\bar{Y})}| \sim 10^{-10} \text{ MeV}^{-\frac{3}{2}}. \quad (44)$$

Of course, we note that this result is dimensional, namely order-of-magnitude estimation and may be off by factors of 10 or more. With this estimated value for the PV coupling constants and order of magnitude of the results of  $c(\bar{X} - \bar{Y})$  in fig.7, the value of  $P_\gamma$  in  $nd \rightarrow {}^3H\gamma$  is estimated as

$$|P_\gamma| \sim 10^{-7}. \quad (45)$$

Experimentally, the  $P_\gamma$  in  $nd \rightarrow {}^3H\gamma$  is not reported up to now at the thermal energy. Therefore we can compare our estimated result with a theoretical methods such as DDH model. The calculated values of  $P_\gamma$  in  $nd \rightarrow {}^3H\gamma$  based on DDH model are given by  $P_\gamma = -1.39 \times 10^{-6}$  and  $P_\gamma = -1.14 \times 10^{-6}$  for two super-soft-core (SSC) and Reid-soft-core (RSC) potentials, respectively [11]. Recently, the value of  $P_\gamma$  in  $nd \rightarrow {}^3H\gamma$  is calculated with the DDH-best parameter values and 4-parameter fits for the different potential models in ref.[12]. The order of magnitude of the results of  $P_\gamma$  in the ref.[12] is the order of  $10^{-7}$ .

We can see that our EFT( $\not{t}$ ) estimation for the  $P_\gamma$  in  $nd \rightarrow {}^3H\gamma$  process at the thermal energy, eq.(45), agrees with the order of other theoretical methods.

## VI. CONCLUSION AND OUTLOOK

In the present EFT( $\not{t}$ ) calculation, the  $P_\gamma$  is calculated in order to minimise the uncertainty in determination of the LECs. We have used the PV two-body interaction in our calculation. No PV three-body interaction is taken into account at the leading order.

The value of the coefficient  $c(\bar{X} - \bar{Y})$  can provide the valuable information in order to use in eq.(43). One can be able to compare eq.(43) with the future experimental value of  $P_\gamma$ . The variation of the coefficient  $c(\bar{X} - \bar{Y})$  indicates that the cutoff dependence is ignorable at the leading order. This small variation can be removed with the consideration of the higher order corrections.

The photon asymmetry  $A_\gamma$  for the neutron-deuteron radiative capture process is an open problem which we are going to calculate it in the near future.

The PV proton-deuteron radiative capture is another process which can help us to identify parity-violating few-body coupling constants. For this process the coulomb interaction should be considered together with the PV and EM interactions, simultaneously.

More challenging reactions such as PV four-body scattering will make the use of EFT more interesting in the future study. This shed light on the accurate evaluation of weak  $dNN$  coupling constants.

### Acknowledgments

The authors would like to thank Harald W. Griebhammer for the valuable  $Nd$  scattering mathematica code. This work was supported by the research council of the University of Tehran.

### Appendix A. THE NORMALIZATION CONDITION FOR THE TRITON WAVE FUNCTION

In order to normalize the triton wave function, one can be able to follow the derivation of the normalization condition for Bethe-Salpeter equation in [21, 22]. We replace the normalization condition of the relativistic two-body BS vertex function  $|\Gamma \rangle$  with the non-relativistic one which is suitable for the  $Nd$  scattering leading to the formation of triton.

One can start from the homogenous equation

$$|\Gamma \rangle = -VG_{BS}|\Gamma \rangle, \quad (\text{A.1})$$

with the normalization condition introduced by Adam *et al.*, [21] as

$$1 = - \langle \Gamma | G_{BS} \frac{\partial}{\partial P^2} (VG_{BS}) \Big|_{P^2=M^2} |\Gamma \rangle, \quad (\text{A.2})$$

where  $V$  denotes the interaction kernel and  $G_{BS}$  represents the BS propagator.  $P$  and  $M$  in eq.(A.2) are total four-momentum of the system and the bound state mass, respectively.

Based on eq.(11), the non-relativistic expression similar to eq.(A.2) can be written as

$$\begin{aligned}
1 = & - \int \frac{d^3q dq_0}{(2\pi)^4} \int \frac{d^3q' dq'_0}{(2\pi)^4} \\
& \times (1 \ 0) (t^{3H}(q))^T \mathcal{D}^{LO}(-B_t + q_0, q) \frac{i}{-q_0 - \frac{q^2}{2m_N} + i\varepsilon} \\
& \times \frac{\partial}{\partial E} \left[ V(E, q, q') \mathcal{D}^{LO}(E + q'_0, q') \right. \\
& \left. \times \frac{i}{-q'_0 - \frac{q'^2}{2m_N} + i\varepsilon} \right] \Bigg|_{E=-B_t} t^{3H}(q') \begin{pmatrix} 1 \\ 0 \end{pmatrix}.
\end{aligned} \tag{A.3}$$

where, after taking into account the energy and solid angle integrations, we have

$$\begin{aligned}
1 = & - \int \frac{q^2 dq}{2\pi^2} \int \frac{q'^2 dq'}{2\pi^2} \\
& \times (1 \ 0) (t^{3H}(q))^T \mathcal{D}^{LO}(-B_t - \frac{q^2}{2m_N}, q) \\
& \times \frac{\partial}{\partial E} \left[ V(E, q, q') \mathcal{D}^{LO}(E - \frac{q'^2}{2m_N}, q') \right] \Bigg|_{E=-B_t} t^{3H}(q') \begin{pmatrix} 1 \\ 0 \end{pmatrix},
\end{aligned} \tag{A.4}$$

where  $t^{3H}(q)$  has been introduced in the text. we Note that  $\begin{pmatrix} 1 \\ 0 \end{pmatrix}$  vector in eq.(A.4) projects  $t^{3H}(q)$  into incoming dibaryon in the deuteron case. Similarly, for the incoming dibaryon in the singlet case,  $\begin{pmatrix} 1 \\ 0 \end{pmatrix}$  and  $(1 \ 0)$  should be replace by  $\begin{pmatrix} 0 \\ 1 \end{pmatrix}$  and  $(0 \ 1)$  in eq.(A.4), respectively. By comparing eq.(11) with (A.1), one can be able to see

$$V(E, q, q') = 2\pi \left[ \mathcal{K}_{(0)}^{PC}(E, q, q') \begin{pmatrix} 1 & -3 \\ -3 & 1 \end{pmatrix} + \mathcal{H}(E, \Lambda) \begin{pmatrix} 1 & -1 \\ -1 & 1 \end{pmatrix} \right]. \tag{A.5}$$

## Appendix B. THE CALCULATION OF $S_1$ AND $S_2$ KERNELS OF THE SET (I) DIAGRAMS

We introduce the contribution of all diagrams in the first and second lines of fig.4 as  $S_{12}$  which is the sum of  $S_1$  and  $S_2$ ,

$$S_{12}(X; E_i, E_f, q) = S_1(X; E_i, E_f, q) + S_2(X; E_i, E_f, q). \quad (\text{B.1})$$

In eq.(B.1),  $X$  and  $q$  are the incoming partial wave and momentum, respectively.  $E_i$  and  $E_f$  are the same as introduced in the text. The  $S_{12}$  can be written in the cluster-configuration space, after applying the energy integration, as

$$\begin{aligned} S_{12}(X; E_i, E_f, q) = & - \int q'^2 dq' t^{3H^\dagger}(q') \left\{ \mathcal{D}^{LO}(E_f - \frac{q'^2}{2m_N}, q') \right. \\ & \left\{ \left[ \mathcal{S}^{A^{up}} + \mathcal{S}^{A^{down}} + \mathcal{S}^{B^{up}} + \mathcal{S}^{B^{down}} + \mathcal{S}^D \right] \right. \\ & \left. + \frac{1}{4\pi^4} \int p^2 dp \tilde{t}^{LO,PV}(Y \rightarrow {}^2S_{\frac{1}{2}}; E_f, p, q') \times \right. \\ & \left. \left. \times \mathcal{D}^{LO}(E_f - \frac{p^2}{2m_N}, p) \left[ \bar{\mathcal{S}}^E + \bar{\mathcal{S}}^F \right] \right\} \right\} \\ & \left. - \mathcal{S}^{C^{up}} - \mathcal{S}^{C^{down}} \right\}, \end{aligned} \quad (\text{B.2})$$

where  $\mathcal{S}^r$  ( $r = A^{up}, A^{down}, B^{up}, B^{down}, C^{up}, C^{down}, D$ ) is a matrix function of  $(X; E_i, E_f, q, q')$  and  $\bar{\mathcal{S}}^{r'}$  ( $r' = E, F$ ) is a matrix function of  $(X \rightarrow Y; E_i, E_f, q, p)$ .

We present the equations of all  $\mathcal{S}^r$  and  $\bar{\mathcal{S}}^{r'}$  in the following for both incoming doublet and quartet partial waves.

### Appendix B.1. The doublet channel ( $X = {}^2S_{\frac{1}{2}}$ )

In this section of Appendix B, we introduce the relations of all  $\mathcal{S}^r$  and  $\bar{\mathcal{S}}^{r'}$  matrix functions for the incoming doublet channel. In the following, we have replaced  $g^{({}^3S_1-{}^1P_1)}$ ,  $g_{\Delta I=0}^{({}^1S_0-{}^3P_0)}$ ,  $g_{\Delta I=1}^{({}^1S_0-{}^3P_0)}$ ,  $g_{\Delta I=2}^{({}^1S_0-{}^3P_0)}$  and  $g^{({}^3S_1-{}^3P_1)}$  by  $g_1, g_2, g_3, g_4$  and  $g_5$ , respectively, as in the text.

After applying the adequate projections for  $X = {}^2S_{\frac{1}{2}}$  channel, in the cluster-configuration

space, the  $\mathcal{S}^{A^{up}}$  and  $\mathcal{S}^{B^{up}}$  are given by

$$\begin{aligned} \mathcal{S}^{A^{up}}(^2S_{\frac{1}{2}}; E_i, E_f, q, q') &= \frac{ey}{24\sqrt{2}} \frac{1}{E_f - E_i} \int \frac{d\Omega_q}{(2\pi)^3} \int \frac{d\Omega_{q'}}{4\pi} \\ &\times \left[ \frac{(2\vec{q}' + \vec{q}) \cdot (\vec{q} + \vec{q}')}{m_N E_i - q^2 - q'^2 - \vec{q} \cdot \vec{q}'} - \frac{(2\vec{q}' + \vec{q}) \cdot (\vec{q} + \vec{q}')}{m_N E_f - q^2 - q'^2 - \vec{q} \cdot \vec{q}'} \right] \\ &\times \begin{pmatrix} (1 - \tau_3)(3g_1 - 2g_5) & -(3 + \tau_3)g_2 + 2(1 + \tau_3)g_3 \\ (3 + \tau_3)(g_1 + 2g_5) & -(3 + 5\tau_3)g_2 - 2(1 + \tau_3)g_3 \end{pmatrix}, \end{aligned} \quad (\text{B.3})$$

$$\begin{aligned} \mathcal{S}^{B^{up}}(^2S_{\frac{1}{2}}; E_i, E_f, q, q') &= \frac{eym_N}{12\sqrt{2}} \int \frac{d\Omega_q}{(2\pi)^3} \int \frac{d\Omega_{q'}}{4\pi} \\ &\times \frac{1}{m_N E_f - q^2 - q'^2 - \vec{q} \cdot \vec{q}'} \begin{pmatrix} 3\tau_3g_1 + 2g_5 & -\tau_3g_2 \\ -\tau_3g_1 - 6g_5 & 3\tau_3g_2 \end{pmatrix}. \end{aligned} \quad (\text{B.4})$$

We can also obtain the  $\mathcal{S}^{A^{down}}$  and  $\mathcal{S}^{B^{down}}$  for the doublet channel by

$$\mathcal{S}^{A(B)^{down}}(^2S_{\frac{1}{2}}; E_i, E_f, q, q') = \left[ \mathcal{S}^{A(B)^{up}}(^2S_{\frac{1}{2}}; E_f, E_i, q', q) \right]^\dagger. \quad (\text{B.5})$$

For all other  $\mathcal{S}^r$  and  $\bar{\mathcal{S}}^{r'}$  matrices, in the incoming doublet channel, we have

$$\begin{aligned} \mathcal{S}^{C^{up}}(^2S_{\frac{1}{2}}; E_i, E_f, q, q') &= \frac{ey}{24\sqrt{2}} \frac{1}{E_f - E_i} \int \frac{d\Omega_q}{(2\pi)^3} \int \frac{d\Omega_{q'}}{4\pi} \\ &\times \left[ \mathcal{D}^{LO}(E_i - \frac{q'^2}{2m_N}, q') \frac{(2\vec{q} + \vec{q}') \cdot \vec{q}'}{m_N E_i - q^2 - q'^2 - \vec{q} \cdot \vec{q}'} \right. \\ &\quad \left. - \mathcal{D}^{LO}(E_f - \frac{q'^2}{2m_N}, q') \frac{(2\vec{q} + \vec{q}') \cdot \vec{q}'}{m_N E_f - q^2 - q'^2 - \vec{q} \cdot \vec{q}'} \right] \\ &\times \begin{pmatrix} (1 + \tau_3)(3g_1 + 2g_5) & -(1 + \tau_3)(3g_2 + 2g_3) \\ (3 - \tau_3)(g_1 + 2g_5) & -(3 - \tau_3)g_2 - 2(1 + \tau_3)g_3 \end{pmatrix}, \end{aligned} \quad (\text{B.6})$$

$$\begin{aligned}
\mathcal{S}^{C^{down}}(^2S_{\frac{1}{2}}; E_i, E_f, q, q') &= \frac{ey}{24\sqrt{2}} \frac{1}{E_f - E_i} \int \frac{d\Omega_q}{(2\pi)^3} \\
&\times \int \frac{d\Omega_{q'}}{4\pi} \left[ \mathcal{D}^{LO}\left(E_i - \frac{q'^2}{2m_N}, q'\right) \frac{(2\vec{q}' + \vec{q}) \cdot \vec{q}'}{m_N E_i - q^2 - q'^2 - \vec{q} \cdot \vec{q}'} \right. \\
&\quad \left. - \mathcal{D}^{LO}\left(E_f - \frac{q'^2}{2m_N}, q'\right) \frac{(2\vec{q}' + \vec{q}) \cdot \vec{q}'}{m_N E_f - q^2 - q'^2 - \vec{q} \cdot \vec{q}'} \right] \\
&\times \begin{pmatrix} (1+\tau_3)(3g_1+2g_5) & (1+\tau_3)(3g_1+2g_5) \\ -(3-\tau_3)g_2+2(1-\tau_3)g_3 & -(3-\tau_3)g_2+2(1-\tau_3)g_3 \end{pmatrix}, \tag{B.7}
\end{aligned}$$

$$\begin{aligned}
\mathcal{S}^D(^2S_{\frac{1}{2}}; E_i, E_f, q, q') &= \frac{ey^3 m_N}{72\sqrt{2}} \frac{1}{E_f - E_i} \int \frac{d^3l}{(2\pi)^3} \int \frac{d\Omega_q}{4\pi} \int \frac{d\Omega_{q'}}{4\pi} \\
&\times \left\{ \left[ \begin{pmatrix} \mathcal{S}_1 & -\mathcal{T} \\ \mathcal{S}_1 & -\mathcal{T} \end{pmatrix} (n_1(E_i, \vec{q}, \vec{l}, \vec{q}') - n_1(E_f, \vec{q}, \vec{l}, \vec{q}')) \right. \right. \\
&\quad \left. \left. + \begin{pmatrix} \mathcal{S}_1 & \mathcal{S}_1 \\ -\mathcal{T} & -\mathcal{T} \end{pmatrix} (n_2(E_i, \vec{q}, \vec{l}, \vec{q}') - n_2(E_f, \vec{q}, \vec{l}, \vec{q}')) \right] \right\}, \tag{B.8}
\end{aligned}$$

$$\begin{aligned}
\bar{\mathcal{S}}^E(^2S_{\frac{1}{2}} \ ^2P_{\frac{1}{2}}; E_i, E_f, q, p) &= -\frac{ey^4 m_N}{48p} \frac{1}{E_f - E_i} \int \frac{d^3l}{(2\pi)^3} \int \frac{d\Omega_q}{4\pi} \int \frac{d\Omega_p}{4\pi} \\
&\times \begin{pmatrix} -1 & 3 \\ 3 & -1 \end{pmatrix} [n_3(E_i, \vec{q}, \vec{l}, \vec{p}) - n_3(E_f, \vec{q}, \vec{l}, \vec{p})], \tag{B.9}
\end{aligned}$$

and

$$\begin{aligned}
\bar{\mathcal{S}}^F(^2S_{\frac{1}{2}} \ ^2P_{\frac{1}{2}}; E_i, E_f, q, p) &= \frac{ey^2}{96q} \frac{1}{E_f - E_i} \int \frac{d\Omega_q}{(2\pi)^3} \int \frac{d\Omega_p}{4\pi} \\
&\times \left[ \frac{(\vec{q} + \vec{p}) \cdot \vec{q}}{m_N E_i - q^2 - p^2 - \vec{q} \cdot \vec{p}} - \frac{(\vec{q} + \vec{p}) \cdot \vec{q}}{m_N E_f - q^2 - p^2 - \vec{q} \cdot \vec{p}} \right] \begin{pmatrix} -3(1-\tau_3) & 3(3+\tau_3) \\ 3(3+\tau_3) & -(3+5\tau_3) \end{pmatrix}. \tag{B.10}
\end{aligned}$$

In the eqs.(B.8) and (B.9) the  $n_1$ ,  $n_2$  and  $n_3$  matrix functions are given by

$$\begin{aligned}
n_1(E, \vec{q}, \vec{l}, \vec{q}') &= \frac{(2\vec{q}' + \vec{l}) \cdot \vec{l}}{m_N E - l^2 - q'^2 - \vec{l} \cdot \vec{q}'} \mathcal{D}^{LO}(E - \frac{q'^2}{2m_N}, q') \\
&\times \left[ \frac{1}{m_N E - q^2 - l^2 - \vec{q} \cdot \vec{l}} \begin{pmatrix} -3(1 + \tau_3) & 9(1 + \tau_3) \\ 3(3 - \tau_3) & -(3 - \tau_3) \end{pmatrix} \right. \\
&\quad \left. + \frac{2H_0(\Lambda)}{\Lambda^2} \begin{pmatrix} 3(1 + \tau_3) & -3(1 + \tau_3) \\ -(3 - \tau_3) & (3 - \tau_3) \end{pmatrix} \right], \\
n_2(E, \vec{q}, \vec{l}, \vec{q}') &= \frac{(\vec{q}' + 2\vec{l}) \cdot \vec{l}}{m_N E - l^2 - q'^2 - \vec{l} \cdot \vec{q}'} \mathcal{D}^{LO}(E - \frac{q'^2}{2m_N}, q') \\
&\times \left[ \frac{1}{m_N E - q^2 - l^2 - \vec{q} \cdot \vec{l}} \begin{pmatrix} -3(1 + \tau_3) & 9(1 + \tau_3) \\ 3(3 - \tau_3) & -(3 - \tau_3) \end{pmatrix} \right. \\
&\quad \left. + \frac{2H_0(\Lambda)}{\Lambda^2} \begin{pmatrix} 3(1 + \tau_3) & -3(1 + \tau_3) \\ -(3 - \tau_3) & (3 - \tau_3) \end{pmatrix} \right], \\
n_3(E, \vec{q}, \vec{l}, \vec{p}) &= \frac{\vec{p} \cdot \vec{l}}{m_N E - l^2 - p^2 - \vec{l} \cdot \vec{p}} \mathcal{D}^{LO}(E - \frac{p^2}{2m_N}, p) \\
&\times \left[ \frac{1}{m_N E - q^2 - l^2 - \vec{q} \cdot \vec{l}} \begin{pmatrix} -3(1 + \tau_3) & 9(1 + \tau_3) \\ 3(3 - \tau_3) & -(3 - \tau_3) \end{pmatrix} \right. \\
&\quad \left. + \frac{2H_0(\Lambda)}{\Lambda^2} \begin{pmatrix} 3(1 + \tau_3) & -3(1 + \tau_3) \\ -(3 - \tau_3) & (3 - \tau_3) \end{pmatrix} \right],
\end{aligned} \tag{B.11}$$

where  $\mathcal{S}_1$  and  $\mathcal{T}$  are introduced previously in sect.III A.

We should emphasize that the contribution of the  $E_3$  diagram in fig.4 is zero because of  $H_0 = 0$  at P-wave ( $L = 1$ ).

### Appendix B.2. The quartet channel ( $X = {}^4S_{\frac{3}{2}}$ )

Similar to the doublet channel, we can write the following equations for the quartet channel. These results are obtained in the cluster-configuration space after applying the adequate incoming and outgoing partial-wave projections. All calculated  $\mathcal{S}^r$  and  $\bar{\mathcal{S}}^{r'}$  matrix

functions in the quartet channel are

$$\begin{aligned}
\mathcal{S}^{A^{up}}(^4S_{\frac{3}{2}}; E_i, E_f, q, q') &= \frac{ey}{12\sqrt{6}} \frac{1}{E_f - E_i} \int \frac{d\Omega_q}{(2\pi)^3} \int \frac{d\Omega_{q'}}{4\pi} \\
&\times \left[ \frac{(2\vec{q}' + \vec{q}) \cdot (\vec{q} + \vec{q}')}{m_N E_i - q^2 - q'^2 - \vec{q} \cdot \vec{q}'} - \frac{(2\vec{q}' + \vec{q}) \cdot (\vec{q} + \vec{q}')}{m_N E_f - q^2 - q'^2 - \vec{q} \cdot \vec{q}'} \right] \\
&\times \begin{pmatrix} (1 - \tau_3)(3g_1 + g_5) & 0 \\ (3 + \tau_3)(g_1 - g_5) & 0 \end{pmatrix},
\end{aligned} \tag{B.12}$$

$$\begin{aligned}
\mathcal{S}^{A^{down}}(^4S_{\frac{3}{2}}; E_i, E_f, q, q') &= \frac{ey}{12\sqrt{6}} \frac{1}{E_f - E_i} \int \frac{d\Omega_q}{(2\pi)^3} \int \frac{d\Omega_{q'}}{4\pi} \\
&\times \left[ \frac{(2\vec{q} + \vec{q}') \cdot (\vec{q} + \vec{q}')}{m_N E_i - q^2 - q'^2 - \vec{q} \cdot \vec{q}'} - \frac{(2\vec{q} + \vec{q}') \cdot (\vec{q} + \vec{q}')}{m_N E_f - q^2 - q'^2 - \vec{q} \cdot \vec{q}'} \right] \\
&\times \begin{pmatrix} -(1 - \tau_3)g_5 & 0 \\ 2(3 + \tau_3)g_2 + 4(1 + \tau_3)g_3 & 0 \end{pmatrix},
\end{aligned} \tag{B.13}$$

$$\begin{aligned}
\mathcal{S}^{B^{up}}(^4S_{\frac{3}{2}}; E_i, E_f, q, q') &= \frac{eym_N}{6\sqrt{6}} \int \frac{d\Omega_q}{(2\pi)^3} \int \frac{d\Omega_{q'}}{4\pi} \\
&\times \frac{1}{m_N E_f - q^2 - q'^2 - \vec{q} \cdot \vec{q}'} \begin{pmatrix} 3\tau_3 g_1 + g_5 & 0 \\ -\tau_3 g_1 + 3g_5 & 0 \end{pmatrix},
\end{aligned} \tag{B.14}$$

$$\begin{aligned}
\mathcal{S}^{B^{down}}(^4S_{\frac{3}{2}}; E_i, E_f, q, q') &= \frac{eym_N}{3\sqrt{6}} \int \frac{d\Omega_q}{(2\pi)^3} \int \frac{d\Omega_{q'}}{4\pi} \\
&\times \frac{1}{m_N E_f - q^2 - q'^2 - \vec{q} \cdot \vec{q}'} \begin{pmatrix} g_5 & 0 \\ \tau_3 g_2 & 0 \end{pmatrix},
\end{aligned} \tag{B.15}$$

$$\begin{aligned}
\mathcal{S}^{C^{up}}(^4S_{\frac{3}{2}}; E_i, E_f, q, q') &= \frac{ey}{12\sqrt{6}} \frac{1}{E_f - E_i} \int \frac{d\Omega_q}{(2\pi)^3} \int \frac{d\Omega_{q'}}{4\pi} \\
&\times \left[ \mathcal{D}^{LO}\left(E_i - \frac{q'^2}{2m_N}, q'\right) \frac{(2\vec{q} + \vec{q}') \cdot \vec{q}'}{m_N E_i - q^2 - q'^2 - \vec{q} \cdot \vec{q}'} \right. \\
&\quad \left. - \mathcal{D}^{LO}\left(E_f - \frac{q'^2}{2m_N}, q'\right) \frac{(2\vec{q} + \vec{q}') \cdot \vec{q}'}{m_N E_f - q^2 - q'^2 - \vec{q} \cdot \vec{q}'} \right] \\
&\times \begin{pmatrix} (1+\tau_3)(3g_1+g_5) & 0 \\ (3-\tau_3)(g_1-g_5) & 0 \end{pmatrix}, \tag{B.16}
\end{aligned}$$

$$\begin{aligned}
\mathcal{S}^{C^{down}}(^4S_{\frac{3}{2}}; E_i, E_f, q, q') &= \frac{ey}{6\sqrt{6}} \frac{1}{E_f - E_i} \int \frac{d\Omega_q}{(2\pi)^3} \int \frac{d\Omega_{q'}}{4\pi} \\
&\times \left[ \mathcal{D}^{LO}\left(E_i - \frac{q'^2}{2m_N}, q'\right) \frac{(2\vec{q}' + \vec{q}) \cdot \vec{q}'}{m_N E_i - q^2 - q'^2 - \vec{q} \cdot \vec{q}'} \right. \\
&\quad \left. - \mathcal{D}^{LO}\left(E_f - \frac{q'^2}{2m_N}, q'\right) \frac{(2\vec{q}' + \vec{q}) \cdot \vec{q}'}{m_N E_f - q^2 - q'^2 - \vec{q} \cdot \vec{q}'} \right] \\
&\times \begin{pmatrix} 2(1+\tau_3)g_5 & 0 \\ (3-\tau_3)g_2 - 2(1-\tau_3)g_3 & 0 \end{pmatrix}, \tag{B.17}
\end{aligned}$$

$$\begin{aligned}
\bar{\mathcal{S}}^F(^4S_{\frac{3}{2}} - ^4P_{\frac{1}{2}}; E_i, E_f, q, p) &= \frac{ey^2\sqrt{3}}{24\sqrt{2}q} \frac{1}{E_f - E_i} \int \frac{d\Omega_q}{(2\pi)^3} \int \frac{d\Omega_p}{4\pi} \\
&\times \left[ \frac{(\vec{q} + \vec{p}) \cdot \vec{q}}{m_N E_i - q^2 - p^2 - \vec{q} \cdot \vec{p}} - \frac{(\vec{q} + \vec{p}) \cdot \vec{q}}{m_N E_f - q^2 - p^2 - \vec{q} \cdot \vec{p}} \right] \\
&\times \begin{pmatrix} (1-\tau_3) & 0 \\ 0 & 0 \end{pmatrix}. \tag{B.18}
\end{aligned}$$

We introduce two contributions in eqs.(B.6-B.10) and (B.16-B.18) for the poles in the nucleon propagators before and after the photon creation, as mentioned in the text. We note that the groups of the diagrams represented by  $D$  and  $E$  in fig.4 have no contribution in the incoming quartet channel because in these diagrams the nucleon which interacts with the photon is a neutron (for  $X = ^4S_{\frac{3}{2}}$  channel) and a photon has no E1 interaction with a neutron.

---

[1] Shi-Lin Zhu, C. M. Maekawa, B. R. Holstein, M. J. Ramsey-Musolf and U. van Kolck, Nucl. Phys. A **748**, 435 (2005).

- [2] M. R. Schindler, R. P. Springer, Prog. Part. Nucl. Phys. **72**, 1 (2013).
- [3] D. R. Phillips, M. R. Schindler and R. P. Springer, Nucl. Phys. A **822**, 1 (2009).
- [4] L. Girlanda, Phys. Rev. C **77**, 067001 (2008).
- [5] J. W. Shin, S. Ando and C. H. Hyun, Phys. Rev. C **81**, 055501 (2010).
- [6] M. R. Schindler and R. P. Springer, Nucl. Phys. A **846**, 51 (2010).[arXiv:nucl-th/0907.5358].
- [7] H. Sadeghi, S. Bayegan and H. W. Griesshammer, Phys. Lett. B **643**, 263 (2006) [arXiv:nucl-th/0610029].
- [8] H. Sadeghi and S. Bayegan, Nucl. Phys. A **753**, 291 (2005).
- [9] H. W. Griesshammer and M. R. Schindler, Eur. Phys. J. A **46**, 73 (2010) [arXiv:nucl-th/10070734].
- [10] H. W. Griesshammer, M. R. Schindler and R. P. Springer, Eur. Phys. J. A **48**, 7 (2012).
- [11] B. Desplanques and J. J. Benayoun, Nucl. Phys. A **458**, 689 (1986).
- [12] Y. Song, R. Lazauskas and V. Gudkov, Phys. Rev. C **86**, 045502 (2012) [arxiv:nucl-th/1207.7039v1].
- [13] A. Avenier *et al.*, Phys. Lett. B **137**, 125 (1984).
- [14] D. R. Phillips, G. Rupak and M. J. Savage, Phys. Lett. B **473**, 209 (2000).
- [15] H. W. Griesshammer, Nucl. Phys. A **744**, 192 (2004).
- [16] P. F. Bedaque, H.-W. Hammer and U. van Kolck, Nucl. Phys. A **676**, 357 (2000).
- [17] R. J. Blin-Stoyle, *Fundamental Interactions and the Nucleus*, (Elsevier, North-Holland, American ,1973).
- [18] J. H. Hetherington and L. H. Schick, Phys. Rev. B **137**, 935 (1965).
- [19] R. T. Cahill and I. H. Sloan, Nucl. Phys. A **165**, 161 (1971).
- [20] R. Aaron and R. D. Amado, Phys. Rev. **150**, 857 (1966).
- [21] J. Adam, Jr., F. Gross, C. Savkli and J.W. Van Orden, Phys. Rev. C **56**, 641 (1997).
- [22] F. Gross, *Relativistic Quantum Mechanics and Field Theory*, (Wiley-Interscience, Virginia, Collage of William and Mary Williamsburg,1993).